

RADIATION FRONT SWEEPING THE AMBIENT MEDIUM OF GAMMA-RAY BURSTS

ANDREI M. BELOBORODOV¹

Stockholm Observatory, SE-133 36, Saltsjöbaden, Sweden; andrei@astro.su.se

Draft version December 2, 2024

ABSTRACT

Prompt emission of gamma-ray bursts (GRBs) is likely generated at early stages of the ejecta expansion, possibly by internal shocks. The γ -ray front overtakes the ejecta and sweeps the ambient medium. As a result a gap is opened between the ejecta and the medium that surfs the front ahead. Effectively, the ejecta move in a cavity until they reach a radius $R_{\text{gap}} \approx 3 \times 10^{15} E_{53}^{1/2}$ cm where E is the isotropic energy of the GRB. At $R = R_{\text{gap}}$ the gap disappears, the blast wave forms and collects the medium behind the radiation front. At radii $R_{\text{gap}} < R < R_{\text{load}} \approx 1.5 \times 10^{16} E_{53}^{1/2}$ cm the blast wave propagates in e^\pm -rich and preaccelerated material. (The medium is e^\pm -loaded in the radiation front: here the scattered GRB photons are decollimated and turn into e^\pm via $\gamma - \gamma$ reaction.) The e^\pm enrichment and preacceleration of the ambient medium should cause a spectacular observational effect: *GRB afterglows should start in optical/UV and evolve fast (< min) to a normal X-ray afterglow*. The early soft emission has an unusual light curve which can overlap with the prompt GRB. If the ambient medium is normal ISM then less than 1% of the blast wave energy is dissipated at the early soft stage. If the medium is a wind from a massive progenitor then almost all the energy is dissipated at this stage. In the massive progenitor scenario, we predict two phenomena: (1) The early soft light curve peaks at $t_{\text{peak}} \approx 12 E_{53}^{1/2}$ s if the Lorentz factor of the ejecta is $\Gamma_{\text{ej}} = 100$ and t_{peak} scales as Γ_{ej}^{-2} . The peak position weakly depends on the wind parameters and offers a way to measure Γ_{ej} . (2) The prompt GRB should have a spectral break at 10 – 100 MeV because harder photons are absorbed by radiation scattered in the wind. The measurement of the break position will determine the wind density.

Subject headings: Cosmology: miscellaneous — gamma-rays: bursts — radiation mechanisms: nonthermal — scattering — shock waves

1. INTRODUCTION

Cosmological gamma-ray bursts (GRBs) are explosions of huge energy $\sim 10^{53}$ ergs, which may be triggered by coalescence of compact objects or collapses of massive stars. The explosion creates a γ -ray pulse with duration of a few seconds that propagates ahead of the explosion ejecta and interacts with the ambient medium first, before the blast wave driven by the ejecta.

Madau & Thompson (2000) and Thomson & Madau (2000, hereafter TM) pointed out that the pulse preaccelerates the medium to a high Lorentz factor. Even more importantly, the pulse-medium interaction is accompanied by runaway loading of e^\pm pairs (TM). The interaction occurs inside the radiation front where the primary photons scatter off the medium and turn into e^\pm pairs via $\gamma - \gamma$ reaction. The created pairs increase the medium opacity, do more scattering, and next generations of e^\pm are created in a runaway manner. TM also discussed the effects of pair loading and preacceleration on the afterglow and suggested that the emission should be softer compared to the standard model (see also recent paper by Mészáros, Ramirez-Ruiz, & Rees 2000). Dermer & Böttcher (2000) discussed the impact of the radiation front on circumstellar clouds.

In the present paper we show that the medium dynamics in the radiation front can be computed in the cold approximation and solve the problem of the front structure. It allows us to assess the impact of the front on the medium and the following

blast wave. In §§ 2 and 3 a detailed formulation of the problem and basic equations are given. Numerical solution is presented in § 4. In § 5 we develop an analytical model that explains the front structure and reproduces the numerical results with good accuracy. The backreaction of the GRB-medium interaction on the prompt γ -rays is studied in § 6. The sweeping of the medium by radiation and the front evolution with radius are studied in § 7. In § 8 we compute the blast wave dynamics in the preaccelerated environment and evaluate its emission.

2. FORMULATION OF THE PROBLEM

2.1. *Basic parameters of the front*

GRB produces a thin shell (“front”) of collimated radiation with bolometric flux $F(\varpi)$ and spectrum $F_\epsilon(\varpi)$ where $\epsilon = h\nu/m_e c^2$ and ϖ is the Lagrangian coordinate in the moving shell, $0 < \varpi < \Delta$. Here Δ is the front thickness and Δ/c is the observed duration of the burst. The front propagates through the ambient medium with velocity c . The medium interaction with the front is convenient to view in the ϖ -coordinate: medium “enters” the Δ -shell at $\varpi = 0$, passes through it and goes out at $\varpi = \Delta$ with new density and velocity. Radiation scattered by the medium is decollimated and also streams towards large ϖ , being absorbed by the primary beam.

The scattering of GRB radiation can have a strong impact on the medium if each electron scatters many photons during its passage through the Δ -shell. The photons “kicked out” by the

¹Also at Astro-Space Center of Lebedev Physical Institute, Profsoyuznaja 84/32, Moscow 117810, Russia

electron from the collimated beam can be converted into e^\pm , so a large number of scatterings would imply a large number of pairs created per one ambient electron. The main contribution to pair production comes from photons with $\epsilon \sim 1$ (see § 5), and their density is $n_{\text{ph}} \sim F/m_e c^3$. The electron scatters many photons in the Δ -shell if the electron “free path” $\lambda = 1/n_{\text{ph}}\sigma_T$ (the difference $\delta\varpi$ between successive scatterings) is smaller than the front width,²

$$\lambda = \frac{m_e c^3}{F \sigma_T} = 4.64 \times 10^6 R_{15}^2 L_{53}^{-1} \text{ cm} < \Delta. \quad (1)$$

The radiation flux is $F = L/4\pi R^2$ where R is the distance from the center of the explosion and L is the isotropic luminosity of the GRB. The total energy of the radiation pulse is $E = (\Delta/c)L$ and the condition (1) can be rewritten as

$$R < R_\lambda = \left(\frac{E \sigma_T}{4\pi m_e c^2} \right)^{1/2} = 8.0 \times 10^{16} E_{53}^{1/2} \text{ cm}. \quad (2)$$

Besides λ there is another important length-scale in the problem of the front structure – the typical $\delta\varpi$ the scattered photons pass before they get absorbed by the primary radiation. This “photon free path” (hereafter denoted $\lambda_{\gamma\gamma}$) far exceeds λ (see § 5). It implies that pair creation occurs at larger ϖ i.e. substantially lags behind scattering. As we show in § 5, the runway pair loading starts at $\varpi = a \approx \sqrt{\lambda \lambda_{\gamma\gamma}} \approx 30\lambda$. The pair loading is efficient if $\Delta > 30\lambda$ which implies a more tight constraint $R < R_{\text{load}} = R_\lambda/\sqrt{30}$. At radii larger than R_{load} there is neither pair loading nor acceleration of the medium.

R_{load} should be compared with the deceleration radius of the GRB ejecta. The standard blast wave model predicts $R_{\text{dec}} \sim 10^{17}$ cm if the ambient medium is normal ISM (with density $\rho_0 \sim 10^{-24} \text{ g cm}^{-3}$) and $R_{\text{dec}} \sim 10^{14} - 10^{16}$ cm if the medium is a wind from a massive progenitor. In the latter scenario, the ambient density and R_{dec} depend on the mass loss \dot{M} and the velocity w of the wind, e.g. $\rho_0 \sim 10^{-18} R_{15}^{-2} \text{ g cm}^{-3}$ and $R_{\text{dec}} \sim 10^{15}$ cm for $\dot{M} = 10^{-5} M_\odot \text{ yr}^{-1}$ and $w = 10^8 \text{ cm s}^{-1}$. $R_{\text{load}} < R_{\text{dec}}$ in the ISM case and then the radiation front affects weakly the blast wave deceleration (but does affect strongly the early emission of the blast wave as we discuss in § 8). We therefore focus more on the massive progenitor scenario where the blast wave is strongly affected by the radiation front. We will show that the standard estimate of R_{dec} is not valid in this case. The correct R_{dec} is found in § 8.

The scattering optical depth of the ambient medium $\tau_R \sim \sigma_T R \rho_0 / m_p$ is very small. Hence the GRB pulse-medium interaction occurs in a specific regime: photons have a low probability of scattering while each electron of the medium experiences a lot of scattering. Pair loading increases the optical depth; in the calculations we assume that the medium stays optically thin and discuss the conditions under which it becomes opaque (§ 6). Radiation in the front strongly dominates over the rest-mass of the ambient medium, $F/c \gg \rho_0 c^2$; the primary radiation dominates over the scattered radiation, e^\pm , and magnetic field.

When the backreaction on the radiation pulse is negligible on time-scales $< R/c$, the propagating $\gamma - e^\pm$ front is *quasi-steady*. It can be formalized as follows. Let us define

$$\varpi = ct - R, \quad (3)$$

where t is the time passed since the beginning of the explosion. Then we have $R = ct$ and $\varpi = 0$ at the leading boundary of

the front, and $\varpi = \Delta$ at the back boundary. Now let us change variables $(t, R) \rightarrow (\varpi, \varpi)$. That the front is quasi-steady means that the medium parameters are functions of $\varpi \ll R$ only and $t \approx R/c$ is a slowly changing parameter. The front gradually changes when its radius R increases. We aim to construct a model for the front structure, i.e. determine the medium density and velocity as functions of ϖ . We will show that the front evolves with time/radius in a self-similar manner: at any t , the density amplification and Lorentz factor of the medium interacting with the radiation pulse depend on one dimensionless variable $\xi = \varpi/\lambda$. Note that the front is thin ($\Delta \ll R$) and its quasi-steady structure (formed on time-scales $\ll R/c$) can be described in plane-parallel geometry.

2.2. Particle collectivization and the cold approximation

The loaded pairs should share immediately their momentum with the medium. There are two possible mechanisms of momentum exchange:

(1) The created e^\pm form a stream that can interact with the medium via beam instability. The instability time-scale is of order ω_{pl}^{-1} where $\omega_{pl} = (4\pi n_e e^2/m_e)^{1/2}$ is the plasma frequency and n_e is the electron density.

(2) In the presence of transverse magnetic field B the pairs gyrate around the field lines frozen into the medium on the Larmor time, $\omega_B^{-1} = m_e c / Be$. The momentum of e^\pm is thus communicated to the medium.

Both mechanisms should work because their time-scales are shorter than the Compton cooling time of e^\pm . The coupling via magnetic field may be dominant if $\omega_B > \omega_{pl}$ which requires $B^2/4\pi > n_e m_e c^2$. When the medium starts to accelerate, one should substitute the rest-frame magnetic field and density in these estimates. The acceleration results in compression (Madau & Thompson 2000), both density and magnetic field are amplified, and the coupling becomes even stronger.

The injected pairs can deposit their momentum into the medium, however, it does not ensure that they also share their energy with other particles before they are Compton cooled. One can therefore distinguish between two situations: (1) *Weak collectivization*: particles injected with a Lorentz factor γ_e (measured in the medium rest frame) get isotropized and preserve γ_e ; the subsequent thermalization of the isotropic particles is controlled by Compton cooling. (2) *Strong collectivization*: all particles share their energy instantaneously and keep a Maxwellian distribution.

We will show that the majority of e^\pm are loaded with moderately relativistic energies, cool efficiently (even with weak collectivization), and remain at non-relativistic energies. Particles created at ϖ are Compton cooled much faster than the medium moves to $\varpi + a$ where next generation of hot pairs is created. Hence the bulk of the pair-creating radiation at $\varpi + a$ has been scattered by cooled particles. To the first approximation, the medium can be considered as a cold plasma with a bulk velocity β found from momentum conservation. We hereafter use this “cold” approximation since it greatly simplifies the calculations; its validity is checked in § 4.

3. BASIC EQUATIONS

In this section we give the equations of a steady radiation front in the plane-parallel geometry (see § 2.1).

²We use the standard notation throughout the paper: a magnitude Y measured in CGS units and divided by 10^k is denoted as Y_k .

3.1. Scattering and pair creation

Let μ be the cosine of the scattering angle. A primary photon scattered through μ starts to move backwards with respect to the Δ -shell with velocity $d\varpi/dt = c(1 - \mu)$, and its ϖ -coordinate grows. The scattering at $0 < \varpi' < \varpi$ determines the intensity of scattered radiation at ϖ ,

$$I_{\text{sc}}(\mu, \epsilon_{\text{sc}}) = \int_0^{\varpi} \frac{d\varpi'}{1 - \mu} F_{\epsilon} n \frac{(1 - \beta)}{2\pi} \frac{d\sigma}{d\mu} \frac{\epsilon_{\text{sc}}}{\epsilon} e^{-\tau_{\gamma\gamma}}. \quad (4)$$

Here $d\varpi'/(1 - \mu) = cdt$ is the length element along the scattered ray, $d\sigma/d\mu$ is Compton cross-section (see Appendix), n is the electron/positron density, and β is the medium velocity in units of c . F_{ϵ} , n , and β are taken at the location of scattering, ϖ' . The photon energies before and after the scattering, ϵ and ϵ_{sc} , are related by

$$\epsilon_{\text{sc}} = \frac{\epsilon(1 - \beta)}{1 - \beta\mu + (1 - \mu)\epsilon/\gamma}, \quad (5)$$

where $\gamma = (1 - \beta^2)^{-1/2}$ is the Lorentz factor of the scattering medium.

The scattered radiation that propagates from ϖ' to ϖ is attenuated by $\gamma - \gamma$ absorption. This is accounted for by the exponential factor in equation (4) where $\tau_{\gamma\gamma}$ is the $\gamma - \gamma$ optical depth,

$$\tau_{\gamma\gamma} = \int_{\varpi'}^{\varpi} \kappa_{\gamma\gamma} d\varpi. \quad (6)$$

The opacity $\kappa_{\gamma\gamma}$ is dominated by the primary collimated radiation (the scattered radiation has much smaller density, see § 2.1). A scattered photon $(\epsilon_{\text{sc}}, \mu)$ can interact with primary photons ϵ that are above the threshold

$$\epsilon_{\text{thr}} = \frac{2}{(1 - \mu)\epsilon_{\text{sc}}}. \quad (7)$$

The cross-section for interaction with $\epsilon \gtrsim \epsilon_{\text{thr}}$ is $\sigma_{\gamma\gamma} \sim 0.1\sigma_{\text{T}}$. The $\tau_{\gamma\gamma}$ can be viewed as the product of $(1 - \mu)\sigma_{\gamma\gamma}$ and the column density of primary photons above the threshold, $\sim s(F_{\epsilon_{\text{thr}}}/m_e c^3)$ where $s = c(t - t') = (\varpi - \varpi')/(1 - \mu)$ is the path passed by the scattered photon.

The exact expression for $\kappa_{\gamma\gamma}(\mu, \epsilon_{\text{sc}})$ is given in equation (7) of Appendix. In numerical examples we will consider a homogeneous primary radiation pulse i.e. assume that the spectrum F_{ϵ} does not depend on ϖ . Then the $\gamma - \gamma$ opacity is homogeneous across the Δ -shell and $\tau_{\gamma\gamma}(\varpi, \varpi') = (\varpi - \varpi')\kappa_{\gamma\gamma}$.

The pair creation rate at given ϖ is determined by the local rate of $\gamma - \gamma$ interaction between $I_{\text{sc}}(\mu, \epsilon_{\text{sc}})$ and the primary beam F_{ϵ} ,

$$\begin{aligned} \dot{n}_{+}(\varpi) &= 2\pi \int_{-1}^1 d\mu \int d\epsilon_{\text{sc}} \frac{I_{\text{sc}}(\mu, \epsilon_{\text{sc}})}{\epsilon_{\text{sc}} m_e c^2} (1 - \mu) \kappa_{\gamma\gamma} \\ &= \int_0^{\varpi} d\varpi' \int_{-1}^1 d\mu \int d\epsilon \frac{d\epsilon_{\text{sc}}}{d\epsilon} \frac{F_{\epsilon} \kappa_{\gamma\gamma}}{\epsilon m_e c^2} n(1 - \beta) \frac{d\sigma}{d\mu} e^{-\tau_{\gamma\gamma}}. \end{aligned} \quad (8)$$

Here we made use of equation (4).

3.2. Continuity equation

Let n_i and n_e be the density of background ions and electrons, and let $2n_{+}$ be the density of created e^{\pm} pairs. The total

electron density of the medium $n = n_e + 2n_{+}$ and its velocity $v = \beta c$ satisfy the continuity equation. For a plane-parallel front the continuity equation reads

$$\frac{\partial n}{\partial t} + \frac{\partial(nv)}{\partial R} = 2\dot{n}_{+} - 2\dot{n}_{\text{ann}}, \quad (9)$$

where \dot{n}_{+} and \dot{n}_{ann} are the local rates of pair creation and annihilation, respectively. The annihilation rate $\dot{n}_{\text{ann}} = (3/8)(1 - \beta^2)n_{+}^2 \sigma_{\text{T}} c$ is many orders of magnitude smaller than \dot{n}_{+} and hereafter we neglect annihilation.

Since both n and v are functions of $\varpi = ct - R$ only, we have $\partial/\partial t = cd/d\varpi$ and $\partial/\partial R = -d/d\varpi$, and rewrite the continuity equation as

$$\frac{d}{d\varpi} [n(1 - \beta)] = 2\dot{n}_{+}. \quad (10)$$

The immediate consequence of this equation is that the magnitude

$$n^* \equiv n(1 - \beta) \quad (11)$$

would conserve in the absence of pair creation and hence the compression of accelerated medium is $(1 - \beta)^{-1}$ (see also Madau & Thompson 2000). In particular, for the background electrons and ions we have

$$n_e^* \equiv n_e(1 - \beta) = n_0, \quad n_i^* \equiv n_i(1 - \beta) = n_{i0}. \quad (12)$$

Here n_0 and n_{i0} are the electron and ion densities prior to the interaction with the front.

The mass density of the medium is (we neglect the additional mass associated with the plasma internal energy: the cold approximation)

$$\rho = n_i m_i + n m_e = \frac{\rho_0}{1 - \beta} \left(1 + \frac{n^*}{n_0} \frac{m_e}{\mu_e m_p} \right), \quad \mu_e \equiv \frac{\rho_0}{n_0 m_p}. \quad (13)$$

We neglected the small contribution ($\sim m_e/m_p$) of the background electrons to ρ_0 . The m_i is the ion mass and μ_e is the medium mass (in units of m_p) per electron: $\mu_e = 1$ for hydrogen and $\mu_e = 2$ for helium or heavier ions. The ratio n^*/n_0 shows the number of e^{\pm} loaded per one background electron.

The cross-section for Compton scattering is inversely proportional to the squared mass of the scatter, so only e^{\pm} are efficient scatters. The average mass per one scatter is

$$m_* = \frac{\rho}{n}. \quad (14)$$

The initial $m_* = \mu_e m_p$ can decrease to m_e as a result of pair loading.

3.3. Momentum conservation

The law of momentum conservation reads (neglecting the pressure forces: the cold approximation)

$$\frac{\partial(v\gamma\rho)}{\partial t} + \frac{\partial(v^2\gamma\rho)}{\partial R} = \dot{P}_{\pm} + \dot{P}_{\text{sc}}, \quad (15)$$

where \dot{P}_{\pm} is the momentum deposited by pair creation per unit volume per unit time and \dot{P}_{sc} is the momentum deposited by photon scattering off the medium. We rewrite this equation as

$$c^2 \frac{d}{d\varpi} [\rho\beta\gamma(1 - \beta)] = \dot{P}_{\pm} + \dot{P}_{\text{sc}}. \quad (16)$$

The scattering passes momentum from the beamed radiation to the medium with rate

$$\dot{P}_{\text{sc}} = \left(1 - \frac{\gamma^4}{\gamma_{\text{sat}}^4}\right) \frac{n^*}{c} \int d\epsilon \frac{F_\epsilon}{\epsilon} \int d\sigma (\epsilon - \mu \epsilon_{\text{sc}}). \quad (17)$$

The factor $1 - \gamma^4/\gamma_{\text{sat}}^4$ accounts for finite collimation angle of the primary radiation (see eq. 6 of Appendix). Assuming that the radiation is emitted by the ejecta with Lorentz factor Γ_{ej} at $R = R_{\text{em}}$, we have $\gamma_{\text{sat}} = \Gamma_{\text{ej}}(R/R_{\text{em}})$ at a radius R .

The momentum deposited by pair creation is given by

$$\dot{P}_\pm = \int_0^\varpi d\varpi' \int_{-1}^1 d\mu \int d\epsilon_{\text{sc}} \frac{F_\epsilon \kappa_{\gamma\gamma}}{\epsilon m_e c^2} n^* \frac{d\sigma}{d\mu} e^{-\tau_{\gamma\gamma}} p_\pm. \quad (18)$$

Here $p_\pm(\mu, \epsilon_{\text{sc}})$ is the average momentum of the e^\pm pair created when a scattered photon $(\mu, \epsilon_{\text{sc}})$ gets absorbed,

$$\frac{p_\pm}{m_e c} = \mu \epsilon_{\text{sc}} + \chi \epsilon_{\text{thr}}. \quad (19)$$

The numerical factor $\chi \sim 1$ is given in equation (9) of Appendix.

3.4. Thermal balance

The continuity and momentum equations allow one to compute the dynamics of the medium in the cold approximation. When we know the dynamics of the cold medium, we can evaluate its temperature from the thermal balance; it will allow us to check the consistency of the cold approximation. The thermal balance in the medium rest frame reads

$$\frac{d(u\tilde{V})}{dt} = -p \frac{d\tilde{V}}{dt} + \gamma_{\text{inj}} m_e c^2 \frac{d(\tilde{n}\tilde{V})}{dt} + (C^+ - C^-) \tilde{V}. \quad (20)$$

Here u is internal energy density of the medium (including rest mass of e^\pm), p is pressure, $\gamma_{\text{inj}}(\varpi)m_e c^2$ is the mean energy of injected e^\pm , \tilde{V} is volume per barion, and $dt = d\tau/\gamma$; all these magnitudes are measured in the rest frame of the medium.

The terms C^\pm are the rates of Compton heating/cooling. Both depend on the particle energy distribution in the medium rest frame. Given the uncertainty of this distribution we replace it by δ -function at a mean Lorentz factor γ_e and estimate roughly

$$C^+ - C^- = \frac{4}{3} (\beta_C^2 \gamma_C^2 - \beta_e^2 \gamma_e^2) \tilde{n} \tilde{V} \sigma_T \tilde{F}_T, \quad (21)$$

where $\gamma_e = \gamma_C$ corresponds to Compton equilibrium and \tilde{F}_T is the flux of (primary) radiation that scatters in Thomson regime; this flux is measured in the medium rest frame and it is approximately

$$\tilde{F}_T = F_T(\epsilon < \epsilon_{\text{KN}}) \frac{1 - \beta}{1 + \beta}, \quad \epsilon_{\text{KN}} \sim \frac{\gamma(1 + \beta)}{\gamma_e}. \quad (22)$$

Here ϵ_{KN} is the typical energy above which the scattering occurs in the Klein-Nishina regime and $F_T(\epsilon < \epsilon_{\text{KN}})$ is the primary flux with $\epsilon < \epsilon_{\text{KN}}$, measured in the lab frame.

The ions carry a small fraction of the thermal energy (even if they manage to share the energy with e^\pm , their density $n_i \ll n$ as soon as pair creation begins) and hence $u \approx \gamma_e m_e c^2 \tilde{n}$. Note

³The ξ -coordinate has the meaning of dimensionless fluence of the burst, $\xi = (\sigma_T/m_e c^3) F \varpi$. The computed $n(\xi)$ and $\gamma(\xi)$ are also the exact solution for bursts with arbitrary light curve $F_1(\varpi)$ once ξ is defined as $\xi = (\sigma_T/m_e c^3) \int_0^\varpi F d\varpi'$.

that $\tilde{n}\tilde{V} = n^*$ and $\tilde{V} = \gamma(1 - \beta)V_0$ where V_0 is volume per barion in the ambient medium prior to interaction with the front. Substituting these relations into equation (20) and taking into account that $d\varpi/d\tilde{t} = c\gamma(1 - \beta)$ we get after simple algebra,

$$\frac{d\gamma_e}{d\varpi} = -\frac{(p/\tilde{n}m_e c^2)}{\gamma(1 - \beta)} \frac{d}{d\varpi} [\gamma(1 - \beta)] + \frac{(\gamma_{\text{inj}} - \gamma_e)}{n^*} \frac{dn^*}{d\varpi} + \frac{4}{3} \frac{(\gamma_C^2 - \gamma_e^2)}{\gamma(1 + \beta)} \frac{\sigma_T F_T}{m_e c^3}. \quad (23)$$

We estimate the pressure interpolating between nonrelativistic $p/\tilde{n}m_e c^2 = (2/3)(\gamma_e - 1)$ and relativistic $p/\tilde{n}m_e c^2 = \gamma_e/3$ limits,

$$\frac{p}{\tilde{n}m_e c^2} \approx \frac{\gamma_e^2 - 1}{3\gamma_e} \approx \frac{kT}{m_e c^2} \equiv \Theta. \quad (24)$$

Here we introduced a temperature T . For a Maxwellian plasma T is related to pressure by $p = \tilde{n}kT$ in both non-relativistic and relativistic cases. For a non-Maxwellian distribution, T is an effective temperature defined by $p = \tilde{n}kT$.

Once we know $\gamma(\varpi)$ and $n^*(\varpi)$ from the dynamic “cold” solution we can find F_T and $\gamma_{\text{inj}}(\varpi)$ (see Appendix). Then we can solve numerically equation (23) and find $\gamma_e(\varpi)$ and $\Theta(\varpi)$.

4. NUMERICAL RESULTS

In this section we construct a numerical model of the front. In the calculations we assume that the ambient medium is hydrogen ($\mu_e = 1$, see eq. 13). In the massive progenitor scenario $\mu_e = 2$ is more appropriate. We will show however, that the solution very weakly depends on μ_e .

We integrate the ordinary differential equations (10) and (16) with the boundary conditions $\beta = 0$ and $n = n_0$ at $\varpi = 0$. At each step $d\varpi$ we know the radiation scattered at previous steps (smaller ϖ) and find the local pair creation rate from equation (8) and the rate of momentum injection from equations (17) and (18). After getting the dynamic solution $n(\varpi)$ and $\gamma(\varpi)$ we integrate the thermal balance equation (23) with the boundary condition $\gamma_e(0) = 1$ and find $\gamma_e(\varpi)$.

The input of the calculations is the GRB spectrum $F_\epsilon(\varpi)$ and the output is the front structure $n(\varpi)$, $\beta(\varpi)$, and $\gamma_e(\varpi)$. For numerical illustration we take a radiation pulse with constant spectrum

$$F_\epsilon = \begin{cases} F_1 \epsilon^{-\alpha_1}, & \epsilon < 1, \\ F_1 \epsilon^{-\alpha_2}, & 1 < \epsilon < \epsilon_{\text{br}}, \\ 0, & \epsilon > \epsilon_{\text{br}}. \end{cases} \quad (25)$$

Such a spectral shape is observed in GRBs with $\alpha_1 \sim \pm 0.5$ and $\alpha_2 \sim 1.5 \pm 0.5$ (Preece et al. 2000). In numerical examples we fix $\alpha_1 = 0$ and assume $\alpha_2 > 1$. Then the problem has a well defined solution in the limit $\epsilon_{\text{br}} \rightarrow \infty$. The finiteness of $\epsilon_{\text{br}} \gg 1$ causes a break in pair loading at $\varpi = \varpi_{\text{br}}$ (see §§ 5.3 and 6). In the examples below we assume $\epsilon_{\text{br}} = 10^2$.

The solution is a function of the dimensionless coordinate³ $\xi = \varpi/\lambda$ where λ is given by equation (1) with the total flux

$$F = \frac{(\alpha_2 - \alpha_1)F_1}{(1 - \alpha_1)(\alpha_2 - 1)}. \quad (26)$$

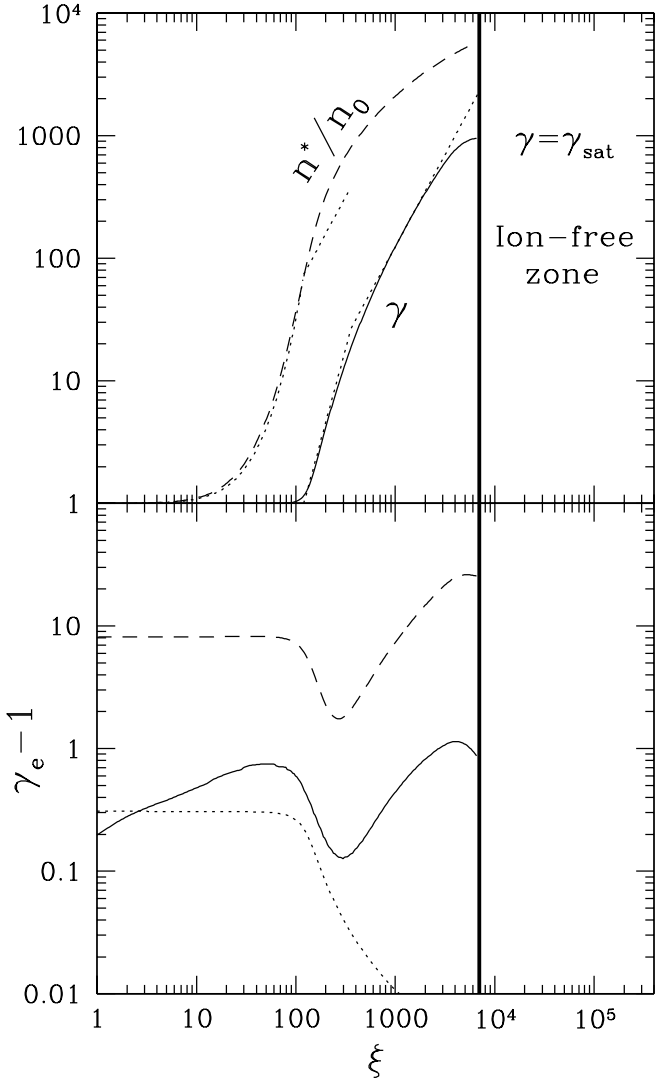


FIG. 1.— Structure of the radiation front for $\alpha_1 = 0$, $\alpha_2 = 1.5$, $\epsilon_{\text{br}} = 10^2$. Top: Dynamic solution. Dashed and solid curves show $n^*(\xi)/n_0$ and $\gamma(\xi)$ where $\xi = \varpi/\lambda$. Solid vertical line shows the boundary of the ion-free zone, ξ_c , where γ reaches γ_{sat} . Dotted curves show the analytical model of § 5 (see eqs. 49,62,63). Bottom: Thermal structure of the front. Solid curve shows the mean kinetic energy of the particles in the medium rest frame, $\gamma_e - 1$. Dashed and dotted curves display $\gamma_{\text{inj}} - 1$ and $\gamma_C - 1$, respectively.

4.1. Dynamical structure of the front

Figure 1 shows the solution for the front structure in the case of $\alpha_2 = 1.5$. The solution does not depend on γ_{sat} until γ approaches γ_{sat} . In Figure 1 $\gamma_{\text{sat}} = 10^3$ is assumed.

At modest ξ (near the leading boundary of the front) the medium is static, $\gamma = 1$, and pair loading proceeds exponentially on scale of $\xi_{\text{load}} \approx 30$. When a portion $d\varpi$ of the radiation pulse overtakes a static electron, it passes momentum $dp = (F_T \sigma_T / c^2) d\varpi$ where $F_T \sim 0.1F$ is the flux of radiation that scatters in Thomson regime. Hence $dp/d\xi \sim 0.1m_e c$ and the medium acceleration length is $\xi_{\text{acc}} \sim 10m_*/m_e$ where $m_* = m_p(n_0/n^*)$ is mass per scatter (see eqs. 14 and 13). This yields an estimate

$$\xi_{\text{acc}} \approx 10(m_p/m_e) \exp(-\xi_{\text{acc}}/30) \quad (27)$$

i.e. $\xi_{\text{acc}} \approx 10^2$. The estimate neglects the additional acceleration due to \dot{P}_\pm which is approximately equal to \dot{P}_{sc} at $\xi \sim \xi_{\text{acc}}$ (see Fig. 2). More exact formulae are derived in § 5.

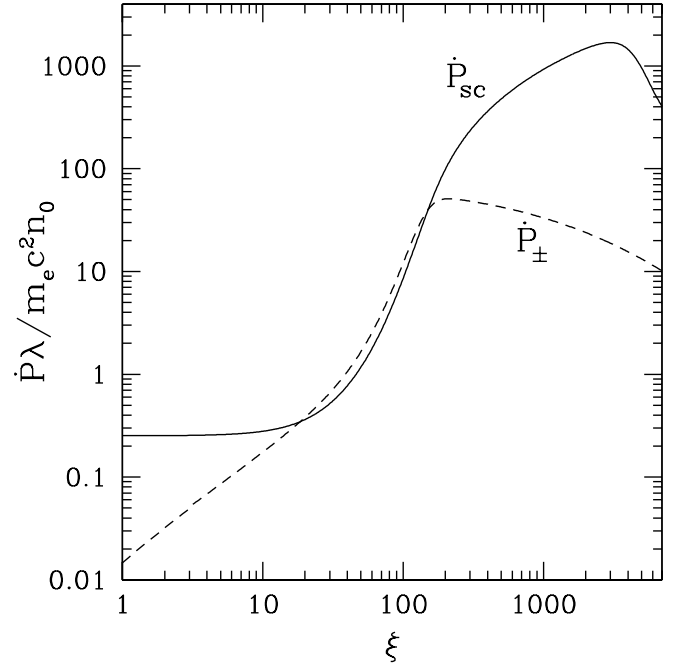


FIG. 2.— Momentum deposition rate for the front shown in Figure 1. Solid and dashed curves display \dot{P}_{sc} and \dot{P}_\pm (see eqs. 16-18).

The pair loading continues in the accelerated zone $\xi > \xi_{\text{acc}}$ and m_* further decreases. Therefore the medium accelerates very fast, $\gamma \approx (\xi/\xi_{\text{acc}})^3$, until n^*/n_0 reaches m_p/m_e and m_* saturates at m_e ; afterwards $\gamma \propto \xi^{3/2}$.

The accelerating medium scatters radiation through smaller angles, $\mu \sim \beta \rightarrow 1$, and pair production slows down ($d^2 n^*/d\xi^2$ becomes negative at $\xi \approx \xi_{\text{acc}}$). The threshold energy for $\gamma - \gamma$ interaction (eq. 7) grows $\epsilon_{\text{thr}} \propto \gamma^2 \propto (\xi/\xi_{\text{acc}})^6$ and the $\gamma - \gamma$ opacity seen by scattered photons, $\kappa_{\gamma\gamma} \propto \epsilon_{\text{thr}}^{-\alpha_2}$, becomes very low. The scattered photons travel almost freely across the front with free-path $\lambda_{\gamma\gamma} = \kappa_{\gamma\gamma}^{-1} \propto (\xi/\xi_{\text{acc}})^{6\alpha_2}$. E.g. photons $\epsilon = 1$ scattered by medium with $\gamma = 2$ at $\xi \gtrsim \xi_{\text{acc}}$ are mostly absorbed only at $\xi > 10^4$, i.e. absorption strongly lags behind scattering. As we explain in § 5, the radiation scattered at $\xi_{\text{acc}} < \xi < 3\xi_{\text{acc}}$ controls pair loading at all reasonable $\xi > \xi_{\text{acc}}$, and the bulk of radiation scattered at $\xi > \xi_{\text{sc}}$ (where $\gamma > \gamma_{\text{sc}} = \sqrt{\epsilon_{\text{br}}}/4$) will never be absorbed. Pair loading thus decouples from the medium dynamics at $\xi \gg \xi_{\text{acc}}$.

At $\xi_\pm \approx 10^3$ the e^\pm density exceeds the density of the ambient electrons by the factor m_p/m_e and m_* saturates at m_e . Then equations (16) and (17) yield

$$\frac{d\gamma}{d\xi} = \frac{1}{2} \left(1 - \frac{\gamma^4}{\gamma_{\text{sat}}^4} \right) - \frac{\gamma}{n^*} \frac{dn^*}{d\xi}. \quad (28)$$

Here we took into account that $\beta \approx 1$ and calculated \dot{P}_{sc} with Thomson cross-section (at $\gamma \gg 1$ the bulk of primary radiation scatters in Thomson regime). We neglected \dot{P}_\pm compared to \dot{P}_{sc} , which is a good approximation at $\gamma \gg 1$ (see Fig. 2). In the absence of pair loading ($d \ln n^* / d \ln \xi \ll 1$), γ would tend to the asymptotics $\gamma = \xi/2$. However, before γ can reach any asymptotics, it saturates at $\gamma_{\text{sat}} = 10^3$. The saturation happens at $\xi = \xi_c \lesssim 10^4$.

Our steady dynamic problem becomes inconsistent when γ saturates. The assumption that the front has the speed of light

and the medium moves with respect to the Δ -shell with velocity $d\varpi/dt = 1 - \beta$ then becomes wrong. The medium reaches the equilibrium velocity β_{sat} such that the net flux of radiation vanishes in the medium rest frame. The β_{sat} is determined by the angular spread of the primary radiation and represents the effective velocity of the radiation pulse. Saturation implies that the ambient (ion) medium gets stuck in the pulse and cannot penetrate the zone $\xi > \xi_c$ – this zone is ion-free. (More exactly, the ions cannot penetrate $\xi > \max\{\xi_c, \xi_{\text{mix}}\}$ where $\xi_{\text{mix}} \sim \gamma_{\text{sat}}^{-2} R/\lambda$, see § 7.1). The trapped ions accumulate with time and surf the pulse.

Radiation scattered by the medium in the process of acceleration partially propagates to the ion-free zone of the front and produce e^\pm with a rate \dot{n}_+ owing to $\gamma - \gamma$ reaction with the primary radiation. A steady $\dot{n}_+(\varpi)$ is established even at very large ϖ on relatively short time-scale $\sim \varpi/(1 - \mu)c$ where $1 - \mu \lesssim (1/2\gamma_{\text{sc}}^2) \sim 0.1$ represents the typical collimation angle of the scattered radiation. The pairs created at $\xi > \xi_c$ acquire the saturated Lorentz factor on length $\sim \xi_c$, and then stay practically static in the ϖ -coordinate and accumulate.

In the real explosion problem the acceleration/loading time of the medium is limited to R/c (the time of side expansion of the GRB pulse). One should compare R/c with the time of acceleration to a given $\gamma < \gamma_{\text{sat}}$. The acceleration is most efficient if $m_* = m_e$ and if further pair loading is slow, $d\ln n^*/d\ln \xi \ll 1$. Then equation (28) reads $d\gamma/dt = (c/\lambda)(1 - \beta)/(1 + \beta) \approx (c/4\gamma^2\lambda)$ and gives $t_{\text{acc}} \approx \gamma^3\lambda/c$. From $t_{\text{acc}} < R/c$ we find $\gamma < \gamma_{\text{max}}$ where

$$\gamma_{\text{max}} \approx \left(\frac{R}{\lambda}\right)^{1/3} = 6 \times 10^2 R_{15}^{-1/3} L_{53}^{1/3}. \quad (29)$$

When $\gamma_{\text{max}} < \gamma_{\text{sat}}$ the boundary of the ion-free zone ξ_c is determined by $\gamma = \gamma_{\text{max}}$ rather than $\gamma = \gamma_{\text{sat}}$. More accurate formulae for ξ_c are given in § 7.2.

At any R , the front structure at $\xi < \xi_c$ is well described by the unique self-similar solution shown in Figure 1. Note that $\lambda \propto R^2$ and hence the front gets “stretched” in ϖ -coordinate as radius grows.

The self-similar solution describes the whole front if its trailing boundary $\xi_\Delta \equiv \Delta/\lambda < \xi_c$. The position of the boundary ξ_Δ in Figure 1 moves to the left with increasing R and becomes smaller than ξ_c at a radius R_c (see § 7).

4.2. Thermal structure of the front

In the bottom panel of Figure 1 one can see two peaks of γ_e at $\xi \approx 70$ and $\xi \approx 4 \times 10^3$. They correspond to the beginning and the end of the medium acceleration. This unusual temperature profile can be understood from equation (23) which we rewrite as

$$\frac{d\gamma_e}{d\xi} = \frac{\Theta}{\xi_{\text{acc}}} + \frac{\gamma_{\text{inj}} - \gamma_e}{\xi_{\text{load}}} - \frac{\gamma_e}{\xi_C}. \quad (30)$$

Here the effective temperature Θ is related to the average Lorentz factor γ_e via equation (24), $\xi_{\text{acc}} = (-d\ln[\gamma(1 + \beta)]/d\xi)^{-1}$ is the acceleration length, $\xi_{\text{load}} = (d\ln n^*/d\xi)^{-1}$ is the pair loading length, and

$$\xi_C = \frac{3}{4} \frac{F}{F_T} \frac{\gamma(1 + \beta)\gamma_e}{\gamma_e^2 - \gamma_C^2} = \begin{cases} \frac{3}{4} \frac{F}{F_T} \frac{\gamma(1 + \beta)}{\gamma_e}, & \gamma_e \gg 1, \\ \frac{3}{4} \frac{F}{F_T} \frac{\gamma(1 + \beta)}{\beta_e^2 - \beta_C^2}, & \beta_e \ll 1, \end{cases} \quad (31)$$

is the length of Compton cooling.

The initial temperature of the medium is low and it gradually rises at small ξ owing to injection of pairs with $\gamma_{\text{inj}} \lesssim 10$. Already at $\xi \sim 3$ the temperature exceeds the Compton equilibrium value Θ_C . Thereafter $\Theta > \Theta_C$ and Compton scattering cools the medium rather than heats. At $\xi \sim \xi_{\text{load}} \sim 30$ the pair density exceeds that of background electrons and begins to exponentiate. One could then expect a large heating rate, however Compton cooling is very efficient and keeps the temperature below $m_e c^2$. The length of Compton cooling is $\xi_C \approx (F/F_T)\epsilon_{\text{KN}} \sim 1$. It is much shorter than ξ_{load} and therefore the cooling compete successfully with the heating. This competition is described by equation

$$\frac{d\gamma_e}{d\xi} \approx \frac{\gamma_{\text{inj}}}{\xi_{\text{load}}} - \frac{\gamma_e}{\xi_C}. \quad (32)$$

Here we neglected the first (adiabatic) term on the right-hand side of equation (30) since it is much smaller than the other two terms. Equation (32) shows that $\gamma_e - 1$ saturates at $\sim \xi_C \gamma_{\text{inj}} / \xi_{\text{load}} \lesssim 1$. This is the first maximum of the temperature profile.

At $\xi \sim \xi_{\text{acc}} \approx 10^2$ the medium begins to accelerate and then the relative velocity between the injected e^\pm stream and the medium decreases. Correspondingly, γ_{inj} , the heating rate, and the medium temperature fall down.

When the medium Lorentz factor reaches $\gamma \sim 10$, the relative velocity between the injected e^\pm stream and the medium vanishes and changes sign. Here γ_{inj} reaches a minimum. Afterwards e^\pm loading tries to *decelerate* the medium (see also § 5.4). The acceleration by scattering, however, dominates and the medium continues to accelerate. Now γ_{inj} rises again (the relative velocity between the injected e^\pm and the medium again increases) and the heating rate and the temperature grow.

The cold approximation is especially good near the minimum of γ_e at $\sim 2\xi_{\text{acc}}$. Here the main scattering occurs (that controls pair loading in the whole accelerated zone of the front).

The energy distribution of e^\pm around the average γ_e depends on details of particle thermalization. In the case of weak collectivization (see § 2.2) a tail exists at energies up to γ_{inj} . The length-scale for Compton cooling of injected e^\pm is $\xi_C(\gamma_{\text{inj}}) \sim (F/F_T)\epsilon_{\text{KN}} \sim 1$ (it does not depend on γ_{inj} or γ because $F_T/F \sim \epsilon_{\text{KN}}$ in the case of $\alpha_1 = 0$). Hence the density of pairs with $\gamma \sim \gamma_{\text{inj}}$ is

$$n_{\text{inj}}^* \sim \frac{dn^*}{d\xi} = \frac{n^*}{\xi_{\text{load}}}, \quad (33)$$

i.e. the density of high-energy particles is $\sim \xi_{\text{load}} \sim 30$ times smaller as compared to cooled particles. Also the energy density of the tail is smaller than that of the “thermal” component.

We conclude that the cold approximation is reasonably good. Note however that we focus on relatively soft spectra $\alpha_2 > 1$ (in contrast, TM took $\alpha_2 = 1$ as a basic case). The case of hard spectra $\alpha_2 \lesssim 1$ is more complicated because the maximum of γ_e at $\xi \lesssim \xi_{\text{acc}}$ becomes essentially relativistic and numerical simulations relaxing the cold approximation will be needed. A relativistically hot plasma scatters preferentially backwards (smaller μ). Note also that \dot{P}_\pm then strongly dominates over \dot{P}_{sc} at $\xi \sim \xi_{\text{acc}}$. We expect however that the front structure will not change qualitatively for hard spectra (it will probably get somewhat “compressed” i.e. pair loading and medium acceleration will take place at smaller ξ).

5. ANALYTICAL MODEL

The medium dynamics in the radiation front can be analyzed with a simplified model that we formulate below. In particular, we derive the characteristic lengths ξ_{load} and ξ_{acc} , get an analytical solution for the front in the non-relativistic ($\beta < 0.5$) zone, and evaluate the pair loading rate in the accelerated zone.

5.1. Formulation

Let us replace the scattering cross-section by

$$\frac{d\sigma}{d\mu} = \sigma_T \delta(\mu - \beta) H(\epsilon_{\text{KN}} - \epsilon), \quad (34)$$

where δ is the Dirac function and H is the Heaviside step function. Here we have made two approximations:

1. Assume that radiation scatters with Thomson cross-section if $\epsilon < \epsilon_{\text{KN}}$ and does not scatter at all if $\epsilon > \epsilon_{\text{KN}}$, where $\epsilon_{\text{KN}} \lesssim 1$ is the energy above which the Klein-Nishina corrections reduce the scattering and subsequent pair creation. We derive in Appendix the effective

$$\epsilon_{\text{KN}} \approx 0.4\gamma(1 + \beta) \quad (35)$$

for calculations of \dot{n}_+ and \dot{P}_{\pm} , and

$$\epsilon_{\text{KN}}^{\text{acc}} \approx 0.7\gamma(1 + \beta) \quad (36)$$

for calculations of \dot{P}_{sc} .

2. Replace the broad distribution of the scattering angles by its average, $\mu = \beta$, i.e. assume that the collimated radiation scatters through 90° ($\tilde{\mu} = 0$) in the medium rest frame. Then we also have

$$\epsilon_{\text{sc}} = \frac{\epsilon}{1 + \beta}. \quad (37)$$

The scattered photons can interact with primary photons of energy $\epsilon > \epsilon_{\text{thr}}$ where the threshold is given by equation (7). In our simplified model equation (7) reads

$$\epsilon_{\text{thr}} = \frac{2(1 + \beta)}{\epsilon(1 - \beta)}. \quad (38)$$

We have $\epsilon_{\text{thr}} > 1$ for any $\epsilon < \epsilon_{\text{KN}}$, i.e. the scattered radiation interacts with the high-energy tail $F_{\epsilon} = F_1 \epsilon^{-\alpha_2}$, $\epsilon > 1$. The $\gamma - \gamma$ opacity of the power-law radiation seen by the scattered photon is (see eq. 10 of Appendix)

$$\kappa_{\gamma\gamma} = \frac{\hat{\phi}(\alpha_2)}{\lambda_1} \left(\frac{\epsilon_{\text{thr}}}{2} \right)^{-\alpha_2} H(\epsilon_{\text{thr}} - \epsilon_{\text{br}}), \quad \lambda_1 = \frac{m_e c^3}{F_1 \sigma_T}. \quad (39)$$

The numerical factor $\hat{\phi}(\alpha)$ can be approximated with high accuracy as (Svensson 1987)

$$\hat{\phi}(\alpha) \approx \frac{7}{12} 2^{-\alpha} (1 + \alpha)^{-5/3}. \quad (40)$$

Hereafter we use notation $\phi \equiv \hat{\phi}(\alpha_2) = 0.045$ and 0.023 for $\alpha_2 = 1.5$ and 2 respectively. Equation (39) is exact for the power-law spectrum and inaccuracies appear only when ϵ_{thr}

approaches the spectral break ϵ_{br} . Given the opacity, we also know the free path of the scattered photons $\lambda_{\gamma\gamma} = \kappa_{\gamma\gamma}^{-1}$,

$$\lambda_{\gamma\gamma} = \frac{\lambda_1}{\phi} \left(\frac{\epsilon_{\text{thr}}}{2} \right)^{\alpha_2}. \quad (41)$$

Finally, let us replace the exponential attenuation of the scattered radiation in equation (4) by the step function $H(1 - \tau_{\gamma\gamma})$. Then equations (8), (18), and (17) read

$$\dot{n}_+ = \frac{\phi c}{\lambda_1^2} \int_0^{\varpi} d\varpi' \frac{n^*(\varpi')}{1 + \beta'} \left(\frac{1 - \beta'}{1 + \beta'} \right)^{\alpha_2} \int_0^{\epsilon_{\text{KN}}} \frac{f_{\epsilon} d\epsilon}{\epsilon^{1 - \alpha_2}} \times H(\epsilon_{\text{max}} - \epsilon) H(\epsilon - \epsilon_{\text{min}}), \quad (42)$$

$$\dot{P}_{\pm} = \frac{\phi c}{\lambda_1^2} \int_0^{\varpi} d\varpi' \frac{n^*(\varpi')}{1 + \beta'} \left(\frac{1 - \beta'}{1 + \beta'} \right)^{\alpha_2} \int_0^{\epsilon_{\text{KN}}} \epsilon^{\alpha_2 - 1} f_{\epsilon} d\epsilon \times p_{\pm} H(\epsilon_{\text{max}} - \epsilon) H(\epsilon - \epsilon_{\text{min}}), \quad (43)$$

$$\dot{P}_{\text{sc}} = \left(1 - \frac{\gamma^4}{\gamma_{\text{sat}}^4} \right) \frac{n^* m_e c^2}{(1 + \beta) \lambda_1} \int_0^{\epsilon_{\text{KN}}^{\text{acc}}} f_{\epsilon} d\epsilon. \quad (44)$$

Here $f_{\epsilon} = F/F_1 = \epsilon^{-\alpha_1}$ if $\epsilon < 1$ and $f_{\epsilon} = \epsilon^{-\alpha_2}$ if $\epsilon > 1$, ϵ_{min} is found from the condition $\epsilon_{\text{thr}} < \epsilon_{\text{br}}$,

$$\epsilon_{\text{min}}(\varpi') = \frac{2}{\epsilon_{\text{br}}} \left(\frac{1 + \beta'}{1 - \beta'} \right), \quad (45)$$

and ϵ_{max} is found from the condition $\tau_{\gamma\gamma} = (\varpi - \varpi') \kappa_{\gamma\gamma} < 1$,

$$\epsilon_{\text{max}}(\varpi') = \left[\frac{\lambda_1}{(\varpi - \varpi') \phi} \right]^{1/\alpha_2} \left(\frac{1 + \beta'}{1 - \beta'} \right). \quad (46)$$

When $\epsilon_{\text{max}} > \epsilon_{\text{br}}$ one should replace the upper limit by ϵ_{br} . This refinement is however not important since ϵ_{br} is anyway far from the scattered peak $\epsilon \sim 1$ that dominates pair loading as we show below.

The formula for p_{\pm} (eq. 11 of Appendix) in our simplified model reads

$$\frac{p_{\pm}}{m_e c} = \frac{\epsilon \beta'}{1 + \beta'} + \frac{(1 + \beta')}{\epsilon(1 - \beta')} \frac{\hat{\phi}(\alpha_2 - 1)}{\hat{\phi}(\alpha_2)}. \quad (47)$$

The ϵ -integrals in equations (42), (43), and (44) depend on the relative positions of ϵ_{min} , ϵ_{max} , ϵ_{KN} , and unity. We now consider two different zones of the front starting from small ϖ .

5.2. Non-relativistic zone ($\beta \ll 1$)

In the non-relativistic zone we have $\epsilon_{\text{min}} \ll \epsilon_{\text{KN}} < 1 < \epsilon_{\text{max}}$ and equations (10) and (42) give

$$\begin{aligned} \frac{dn}{d\varpi} &= \frac{2\dot{n}_+}{c} = \frac{2\phi}{\lambda_1^2} \int_0^{\varpi} d\varpi' n(\varpi') \int_{\epsilon_{\text{min}}}^{\epsilon_{\text{KN}}} \epsilon^{\alpha_2 - 1} f_{\epsilon} d\epsilon \\ &= \frac{2\phi \epsilon_{\text{KN}}^{\alpha_2 - \alpha_1}}{\lambda_1^2 (\alpha_2 - \alpha_1)} \int_0^{\varpi} n(\varpi') d\varpi'. \end{aligned} \quad (48)$$

Here we neglected ϵ_{min} compared to ϵ_{KN} . The exact solution of equation (48) is the sum of growing and decaying exponentials,

$$n = \frac{n_0}{2} \left(e^{\varpi/a} + e^{-\varpi/a} \right), \quad \frac{a}{\lambda_1} = \left(\frac{\alpha_2 - \alpha_1}{2\phi \epsilon_{\text{KN}}^{\alpha_2 - \alpha_1}} \right)^{1/2}. \quad (49)$$

Substituting $\alpha_1 = 0$ and $\epsilon_{\text{KN}} = 0.4$ we get $\xi_{\text{load}} = a/\lambda \approx 24$ and 33 for $\alpha_2 = 1.5$ and 2 respectively (here we used $\lambda_1/\lambda = F/F_1$ given by eq. 26). The analytical solution is in perfect agreement with the numerical results, see Figures 1 and 3.

The loading length admits easy interpretation. As seen from equation (48), scattered photons with $\epsilon \sim \epsilon_{\text{KN}}$ make the dominant contribution to \dot{n}_+ . Equations (41) and (38) give the free-path of these photons,

$$\lambda_{\gamma\gamma} \approx \frac{\lambda_1}{\phi} \epsilon_{\text{KN}}^{-\alpha_2}. \quad (50)$$

One can see that $a \approx \sqrt{\lambda_{\gamma\gamma} \lambda_1} \approx \sqrt{\lambda_{\gamma\gamma} \lambda}$. Note that $\lambda_{\gamma\gamma}/\lambda \sim 200$ and 500 for $\alpha_2 = 1.5$ and 2 respectively, i.e. the scattered radiation is weakly absorbed in the static zone (this is a consequence of $\epsilon_{\text{KN}} < \epsilon_{\text{max}}$). At given ϖ , the number of photons scattered by one ambient electron is $\sim \varpi/\lambda$ and a fraction $\sim \varpi/\lambda_{\gamma\gamma}$ of these photons is absorbed. Hence one pair is injected per one ambient electron when $(\varpi/\lambda) \times (\varpi/\lambda_{\gamma\gamma}) = 1$ which gives the above formula for the loading length a .

We now evaluate the medium acceleration at $\beta \ll 1$. Substituting p_{\pm} from equation (47) into equation (18) we get

$$\begin{aligned} \dot{P}_{\pm} &= \frac{\phi m_e c^2}{\lambda_1^2} \int_0^{\varpi} d\varpi' n(\varpi') \int_{\epsilon_{\min}}^{\epsilon_{\text{KN}}} d\epsilon \epsilon^{\alpha_2-2} f_{\epsilon} \frac{\hat{\phi}(\alpha_2-1)}{\hat{\phi}(\alpha_2)} \\ &= \frac{\hat{\phi}(\alpha_2-1) m_e c^2 \epsilon_{\text{KN}}^{\alpha_2-\alpha_1-1}}{2\lambda_1^2(\alpha_2-\alpha_1-1)} n_0 a \left(e^{\varpi/a} - e^{-\varpi/a} \right). \end{aligned} \quad (51)$$

This is a perfect approximation if $\epsilon_{\text{br}} \rightarrow \infty$. The ϵ -integral in (51) peaks at the upper limit as $\epsilon_{\text{KN}}^{\alpha_2-\alpha_1-1}$. Taking $\epsilon_* \sim \epsilon_{\text{KN}}/2$ as a typical ϵ we get the mean energy of absorbed primary photons $\epsilon_{\text{abs}} \approx \chi \epsilon_{\text{thr}} \approx (1 + \alpha_2^{-1})^{5/3} (2/\epsilon_*) \approx 20$. At modest α_2 (hard spectra) low-energy photons $\epsilon \ll \epsilon_{\text{KN}}$ contribute a lot to \dot{P}_{\pm} (they interact with energetic photons $\epsilon_{\text{abs}} \approx 10\epsilon_{\text{KN}}/\epsilon$). Then the finiteness of ϵ_{br} is important – the break suppresses the contribution of photons ϵ for which $\epsilon_{\text{abs}} > \epsilon_{\text{br}}$. E.g. in the case of $\alpha_2 = 1.5$ and $\epsilon_{\text{br}} = 10^2$ the actual \dot{P}_{\pm} is suppressed by a factor of 2 compared to equation (51).

Equation (44) gives a perfect approximation to \dot{P}_{sc} in the non-relativistic zone,

$$\dot{P}_{\text{sc}} = \frac{m_e c^2}{\lambda_1} \frac{(\epsilon_{\text{KN}}^{\text{acc}})^{\alpha_1+1}}{\alpha_1+1} \frac{n_0}{2} \left(e^{\varpi/a} + e^{-\varpi/a} \right). \quad (52)$$

The medium accelerates according to momentum equation (16). With $\gamma \approx 1$ and $\rho \approx \rho_0$ this equation reads

$$\rho_0 c^2 \frac{d\beta}{d\varpi} = \dot{P}_{\pm} + \dot{P}_{\text{sc}}. \quad (53)$$

Substituting (51) and (52) and integrating for β we get

$$\begin{aligned} \beta &= \frac{m_e a}{2\mu_e m_p \lambda_1} \left[\frac{\hat{\phi}(\alpha_2-1) \epsilon_{\text{KN}}^{\alpha_2-\alpha_1-1} a}{(\alpha_2-\alpha_1-1)\lambda_1} \left(e^{\varpi/a} + e^{-\varpi/a} - 2 \right) \right. \\ &\quad \left. + \frac{(\epsilon_{\text{KN}}^{\text{acc}})^{\alpha_1+1}}{\alpha_1+1} \left(e^{\varpi/a} - e^{-\varpi/a} \right) \right]. \end{aligned} \quad (54)$$

Here we used $\rho_0/n_0 = \mu_e m_p$ (see eq. 13). The non-relativistic zone ends when β reaches ~ 0.5 . Equating $\beta = 0.5$ and neglecting the decaying exponential we get the acceleration length

(with $\alpha_1 = 0$, $\epsilon_{\text{KN}} = 0.4$, and $\epsilon_{\text{KN}}^{\text{acc}} = 0.7$),

$$\frac{\varpi_{\text{acc}}}{a} \approx \ln \frac{(\mu_e m_p/m_e)(\lambda_1/a)}{\frac{\hat{\phi}(\alpha_2-1) \epsilon_{\text{KN}}^{\alpha_2-1}}{(\alpha_2-1)}(a/\lambda_1) + 0.7} \approx 5 + \ln \mu_e. \quad (55)$$

Hence $\xi_{\text{acc}} \approx 5\xi_{\text{load}}$ at $\mu_e = 1$, in full agreement with the numerical simulations (Fig. 1 and 3). As one can see from equation (55), with $\mu_e = 2$ the result changes only slightly, $\xi_{\text{acc}} \approx 5.7\xi_{\text{load}}$. Note that ξ_{load} does not depend on μ_e at all. Hence the front structure is not sensitive to the chemical composition of the ambient medium.

5.3. Relativistic zone ($\beta \rightarrow 1$)

At $\varpi > \varpi_{\text{acc}}$ the medium continues to accelerate relativistically. Then ϵ_{KN} grows (eq. 35) and exceeds unity. The integral over ϖ' in equations (42) and (43) is now taken over two regions: $0 < \varpi' < \varpi_1$ where $\epsilon_{\text{max}}(\varpi') < 1$ and $\varpi_1 < \varpi' < \varpi$ where $\epsilon_{\text{max}}(\varpi') > 1$. The boundary ϖ_1 is defined by condition $\epsilon_{\text{max}} = 1$,

$$\varpi - \varpi_1 = \frac{\lambda_1}{\phi} \left(\frac{1 + \beta_1}{1 - \beta_1} \right)^{\alpha_2}. \quad (56)$$

This is an implicit equation for ϖ_1 where $\beta_1 = \beta(\varpi_1)$. One can show that $\varpi_{\text{acc}} < \varpi_1 \ll \varpi$ when $\gamma(\varpi) \gg 1$. From equation (42) we then find

$$\begin{aligned} \dot{n}_+ &= \frac{\phi c}{\lambda_1^2} \int_0^{\varpi} d\varpi' \frac{n^*(\varpi')}{1 + \beta'} \left(\frac{1 - \beta'}{1 + \beta'} \right)^{\alpha_2} Q(\varpi'), \\ Q(\varpi') &= \begin{cases} \frac{\epsilon_{\text{max}}^{\alpha_2-\alpha_1}}{\alpha_2-\alpha_1}, & \varpi' < \varpi_1, \\ \frac{1}{\alpha_2-\alpha_1} + \ln \min\{\epsilon_{\text{max}}, \epsilon_{\text{KN}}\}, & \varpi' > \varpi_1. \end{cases} \end{aligned} \quad (57)$$

The integral peaks at $\varpi' \sim \varpi_1$ (where $\epsilon_{\min} \ll \epsilon_{\text{max}} \sim 1$ and we therefore set $\epsilon_{\min} \approx 0$ in the expression for Q). Denote the integrand as S and evaluate the integral as $\int d\varpi' S \approx \zeta \varpi_1 S(\varpi_1)$. We have $S \propto n^*$ at $\varpi' < \varpi_1$ and a steep decline $S \propto n^*(\gamma')^{2\alpha_2}$ at $\varpi' > \varpi_1$, hence $\zeta \approx (d \ln n^* / d \ln \varpi + 1)^{-1}$. From the numerical results we see that $\zeta \approx 1/3$. Then we get

$$\dot{n}_+(\varpi) \sim \frac{\zeta c n_1^* \varpi_1}{(\alpha_2 - \alpha_1) \lambda_1 (\varpi - \varpi_1)}. \quad (58)$$

This formula gives a reasonable approximation to \dot{n}_+ at $\varpi > \varpi_{\text{acc}}$ (see Fig. 3).

The approximation $\epsilon_{\min} \ll 1$ used in the derivation of equation (58) breaks when $\epsilon_{\min}(\varpi_1)$ approaches unity i.e. ϵ_{thr} for scattered photons with $\epsilon = 1$ approaches ϵ_{br} . We define a typical ϖ_{sc} such that $\epsilon_{\min}(\varpi_1 = \varpi_{\text{sc}}) = 1/2$ (i.e. $\epsilon_{\text{thr}} = \epsilon_{\text{br}}/2$). The velocity of scattering medium at ϖ_{sc} is given by (see eq. 45)

$$\frac{1 + \beta_{\text{sc}}}{1 - \beta_{\text{sc}}} = \frac{\epsilon_{\text{br}}}{4}, \quad \gamma_{\text{sc}} \approx \frac{\sqrt{\epsilon_{\text{br}}}}{4} \quad \text{if } \epsilon_{\text{br}} > 100. \quad (59)$$

At $\varpi_1 > \varpi_{\text{sc}}$ the scattered peak $\epsilon \sim 1$ does not get absorbed at any ϖ . The corresponding cut off in pair loading appears at

$$\varpi_{\text{br}} = \frac{\lambda_1}{\phi} \left(\frac{\epsilon_{\text{br}}}{4} \right)^{\alpha_2} \sim \varpi_{\text{acc}} \left(\frac{\epsilon_{\text{br}}}{4} \right)^{\alpha_2}. \quad (60)$$

We conclude that (1) pair loading at any ϖ is sensitive to the medium dynamics at $\varpi < \varpi_{\text{sc}}$ only and (2) the extension of the pair loading zone is limited by finite ϵ_{br} .

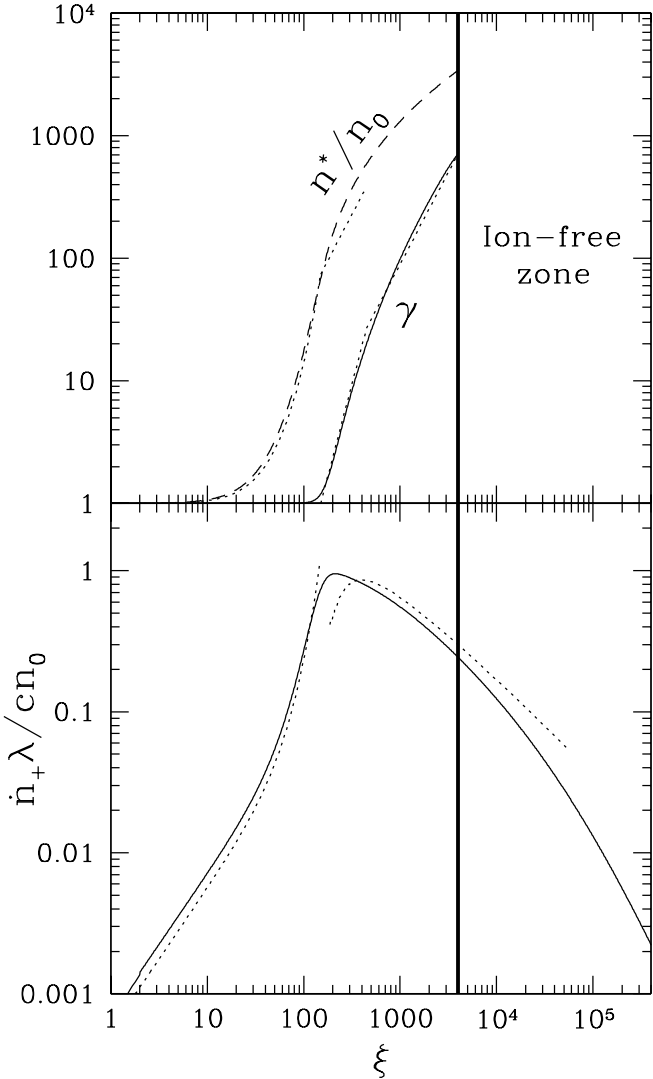


FIG. 3.— Comparison of the analytical model (dotted curves) with the exact numerical results for $\alpha_2 = 2$ and $\epsilon_{\text{br}} = 10^2$. Here $\xi_{\text{load}} \approx 30$ (see eq. 49). The break in \dot{n}_+ is at $\xi_{\text{br}} \sim 5 \times 10^4$. The boundary of the ion-free zone ξ_c is shown by solid vertical line. In this example, $\xi_c = 4 \times 10^3$ is chosen close to its typical value (see § 7).

The simple qualitative picture of pair loading in the relativistic zone is as follows. The scattering of photons with $\epsilon \sim \epsilon_{\text{max}} \sim 1$ makes dominant contribution to \dot{n}_+ at any $\varpi < \varpi_{\text{br}}$. Photons scattered at a given $\varpi_1 > \varpi_{\text{acc}}$ get absorbed at $\varpi = \varpi_1 + \lambda_{\gamma\gamma} \approx \lambda_{\gamma\gamma}$ where

$$\lambda_{\gamma\gamma} \sim \varpi_{\text{acc}} \left(\frac{1 + \beta_1}{1 - \beta_1} \right)^{\alpha_2}, \quad \beta_1 > 0.5. \quad (61)$$

The transition from the regime $\lambda_{\gamma\gamma} \gg \varpi$ found in the non-relativistic zone to the regime $\lambda_{\gamma\gamma} \approx \varpi$ happens at a few ϖ_{acc} . The scattering in a narrow interval $\xi_{\text{acc}} < \xi < 3\xi_{\text{acc}}$ controls pair loading in the whole relativistic zone $\xi_{\text{acc}} < \xi < 10^8$. Unfortunately, we do not have any simple analytical solution at $\xi_{\text{acc}} < \xi < 3\xi_{\text{acc}}$. Looking at the exact numerical solution we see that the formula

$$\gamma = \begin{cases} \left(\frac{\xi}{\xi_{\text{acc}}} \right)^3, & \xi_{\text{acc}} < \xi < 3\xi_{\text{acc}}, \\ 3\sqrt{3} \left(\frac{\xi}{\xi_{\text{acc}}} \right)^{3/2}, & \xi > 3\xi_{\text{acc}} \end{cases} \quad (62)$$

is a perfect approximation for both $\alpha_2 = 1.5$ and $\alpha_2 = 2$ (Fig. 1 and 3). n^*/n_0 can be roughly approximated as

$$\frac{n^*}{n_0} \sim \frac{n_{\text{acc}}^*}{n_0} \left(\frac{\xi}{\xi_{\text{acc}}} \right)^2 \approx 75 \left(\frac{\xi}{\xi_{\text{acc}}} \right)^2, \quad \xi_{\text{acc}} < \xi < 3\xi_{\text{acc}}. \quad (63)$$

Here we have substituted $n_{\text{acc}}^* = n^*(\xi_{\text{acc}}) = 75n_0$ as we know from the non-relativistic solution.

5.4. Heating by pair loading

In the lab frame, the energy and momentum of a created e^\pm pair is dominated by the absorbed primary (collimated) photon,

$$\frac{e_\pm}{m_e c^2} \approx \frac{p_\pm}{m_e c} \approx \epsilon_{\text{abs}} = \chi \epsilon_{\text{thr}}. \quad (64)$$

Here we used equation (11) of Appendix. This expression can be further averaged over the spectrum of scattered photons. The averaged values can be written as $e_\pm/c \approx p_\pm \approx \dot{P}_\pm/\dot{n}_+$.

In the non-relativistic zone we have $\gamma_{\text{inj}} - 1 = e_\pm/2m_e c^2$. The loaded e^\pm push the medium forward and heat it. Using equations (42) and (43) we get

$$\gamma_{\text{inj}} - 1 = \frac{\dot{P}_\pm}{2\dot{n}_+ m_e c} = \frac{(1 + \alpha_2^{-1})^{5/3}(\alpha_2 - \alpha_1)}{(\alpha_2 - \alpha_1 - 1)\epsilon_{\text{KN}}}. \quad (65)$$

For hard spectra and modest ϵ_{br} this equation overestimates γ_{inj} (see discussion after eq. 51). E.g. for $\alpha_2 = 1.5$ and $\epsilon_{\text{br}} = 10^2$ the actual $\gamma_{\text{inj}} \approx 10$ (twice as small).

In the relativistic zone, $\xi \gg \xi_{\text{acc}}$, we have

$$\frac{e_\pm}{2m_e c^2 \gamma} = \frac{\chi \epsilon_{\text{thr}}}{2\gamma} \approx \frac{1}{\gamma} \left(\frac{\phi \varpi}{\lambda_1} \right)^{1/\alpha_2} \sim \frac{0.1 \xi^{1/\alpha_2}}{\gamma} \ll 1, \quad (66)$$

i.e. the e^\pm loading decelerates the medium. Same effect can be viewed from the medium rest frame. We use equations (11) and (12) of Appendix and substitute $\mu = \beta_1$, $\epsilon_{\text{sc}} = (1 + \beta_1)^{-1}$, and $\epsilon_{\text{thr}} = 2(1 + \beta_1)/(1 - \beta_1)$ (cf. §§ 5.1 and 5.3). Then we find the Lorentz factor of created e^\pm in the rest frame,

$$\gamma_{\text{inj}} = \frac{\gamma}{2} [\epsilon_{\text{sc}}(1 - \beta\beta_1) + \chi \epsilon_{\text{thr}}(1 - \beta)] \approx \frac{\gamma}{\epsilon_{\text{thr}}} + \frac{\chi \epsilon_{\text{thr}}}{4} \approx \frac{\gamma}{\epsilon_{\text{thr}}} \gg 1, \quad (67)$$

where we used $\gamma \gg \gamma_1$. Here we keep only the ϵ_{sc} term and neglect the ϵ_{abs} term: the scattered photon is more energetic [being blueshifted as $\gamma(2\gamma_1^2)^{-1} > 1$] than the primary collimated photon [redshifted as $(2\gamma)^{-1}$].

In a similar way we evaluate the momentum per injected particle as viewed from the rest frame of the medium,

$$p_{\text{inj}} \sim \begin{cases} \epsilon_{\text{thr}}, & \xi < \xi_{\text{acc}}, \\ -\gamma/\epsilon_{\text{thr}}, & \xi \gg \xi_{\text{acc}}. \end{cases} \quad (68)$$

At $\xi \gtrsim \xi_{\text{acc}}$ p_{inj} changes sign. Here $\epsilon_{\text{thr}}/\gamma \sim 1$ and $\gamma_{\text{inj}} \sim (\epsilon_{\text{thr}}/\gamma) + (\gamma/\epsilon_{\text{thr}})$ reaches its minimum ~ 2 (see Fig. 1).

Pairs injected in the relativistic zone with $e_\pm \ll 2m_e c^2 \gamma$ tend to acquire the bulk γ . In the case of weak collectivization (cf. § 2.2) this is achieved by radiative acceleration and the e^\pm form a distribution $dn/d\gamma' \propto (\gamma')^2$ at $e_\pm/2m_e c^2 < \gamma' < \gamma$. When the created e^\pm begin to accelerate they produce scattered radiation within angle $(1 - \mu) \sim (e_\pm/m_e c^2)^{-2} = (\chi \epsilon_{\text{thr}})^{-2}$. This radiation can interact with the primary beam and produce secondary pairs if the new threshold $\sim 4/(1 - \mu)$ is less than $\sim \epsilon_{\text{br}}/2$, which would require $\epsilon_{\text{thr}} < \sqrt{\epsilon_{\text{br}}}/4\chi$. Hence at $\epsilon_{\text{br}} < 10^3$ there is no secondary pair production.

6. BACKREACTION ON GRB

6.1. Scattering

The scattering in the front can affect the observed GRB if the medium has a substantial optical depth. In all calculations we assumed that the medium stays optically thin after pair loading. We now address this assumption.

Consider a radius R and let the ambient medium have optical depth $\tau_R = n_0(R)\sigma_T R$ at this radius. In constant density medium with density n_0 ,

$$\tau_R = 7 \times 10^{-10} R_{15} n_0. \quad (69)$$

In a wind with mass loss rate \dot{M} and velocity w ,

$$\tau_R = 3 \times 10^{-4} R_{15}^{-1} \frac{\dot{M}_{21}}{\mu_e w_8}. \quad (70)$$

The pair loading in the radiation front increases the optical depth of the medium. The optical depth seen by the primary photons at given ϖ is

$$\tau_R^* = \tau_R \frac{n^*(\varpi)}{n_0}. \quad (71)$$

Suppose τ_R^* reaches unity at some ϖ_{cr} . Radiation scatters here off the medium with $\gamma_{\text{cr}} = \gamma(\varpi_{\text{cr}})$ and acquires a new collimation angle $\theta \sim \gamma_{\text{cr}}^{-1}$. This decollimation is not crucial if γ_{cr} is sufficiently large, $\gamma_{\text{cr}} > \gamma_{\text{min}} \sim 10^2 - 10^3$. From the solution for n^*/n_0 and γ (Fig. 1 and 3) one sees that the condition $\tau_R^* < 1$ at $\gamma = \gamma_{\text{min}}$ reads

$$\tau_R < \tau_{\text{cr}} \sim (0.3 - 1) \times 10^{-3}. \quad (72)$$

This constraint weakly depends on the exact choice of γ_{min} in the range $10^2 - 10^3$.

A large fraction of the burst can be affected by scattering at $R > R_c$ (at smaller radii the medium interacts only with a small leading portion of the GRB, see § 7). Throughout the paper we assume that $\tau_R < \tau_{\text{cr}}$ at $R > R_c$. In the ISM case ($n_0 = \text{const} \sim 1 \text{ cm}^{-3}$) this condition is satisfied for any reasonable parameters. In the wind case the condition $\tau_R(R_c) < \tau_{\text{cr}}$ reads (for short burst, cf. § 7.2, eq. 93)

$$\frac{\dot{M}_{21}}{\mu_e w_8} < 3 E_{53}^{3/7} t_b^{1/7}. \quad (73)$$

6.2. $\gamma - \gamma$ absorption and the high-energy break

In previous sections we assumed *a priori* a high-energy break in the primary radiation spectrum at ϵ_{br} . In a self-consistent situation, ϵ_{br} is determined by $\gamma - \gamma$ absorption of the primary γ -rays by the scattered radiation field. One can evaluate ϵ_{br} in a simple way. At given ϖ the primary photons $\epsilon \sim \epsilon_{\text{thr}}$ are absorbed with rate $\dot{n}_+(\varpi)$. The number of absorbed photons during time R/c should not exceed the available number of primary photons. This condition reads $\dot{n}_+(R/c) < (F_1/m_e c^3) \epsilon_{\text{thr}}^{-\alpha_2-1}$ and gives the upper limit on ϵ_{thr} i.e. the self-consistent ϵ_{br} . Using equation (58) and the condition $(\varpi \phi/\lambda_1) \epsilon_{\text{thr}}^{-\alpha_2} = 1$ ($\epsilon_{\text{max}} = 1$, see § 5.3) we get (omitting a numerical factor ~ 1)

$$\epsilon_{\text{thr}} < \frac{\xi_{\text{acc}}}{\xi_1} \frac{1}{n_1^* R \sigma_T} = \frac{\xi_{\text{acc}}}{\xi_1} \frac{n_0}{n_1^*} \frac{1}{\tau_R}. \quad (74)$$

Hence $\epsilon_{\text{br}} > 1$ if $\tau_R(n_{\text{acc}}^*/n_0) < 1$, i.e. the main radiation $\epsilon \sim 1$ is not self-absorbed after scattering if

$$\tau_R < \frac{n_0}{n_{\text{acc}}^*} \approx 10^{-2}. \quad (75)$$

This condition is weaker than the transparency condition (71). To find ϵ_{br} at $\tau_R < 10^{-2}$ we need to solve the inequality (74) which is implicit since ϵ_{thr} is a function of ξ_1 . The solution gives the maximum ξ_1^{max} and the corresponding $\epsilon_{\text{thr}}^{\text{max}} = \epsilon_{\text{br}}$. At $\tau_R \ll 10^{-2}$ we have $\epsilon_{\text{br}} \gg 1$; then $\epsilon_{\text{thr}} \approx 8 \gamma_1^2 = 8(\xi_1/\xi_{\text{acc}})^6$ and $n_1^* = 75 n_0 (\xi_1/\xi_{\text{acc}})^2$ (using eqs. 62 and 63). We thus find $\xi_1^{\text{max}}/\xi_{\text{acc}} = (600 \tau_R)^{1/9}$ and

$$\epsilon_{\text{br}} \approx 0.1 \tau_R^{-2/3}, \quad \tau_R \ll 10^{-2}. \quad (76)$$

The break appears in the GRB if $\varpi_{\text{br}} < \Delta$ where ϖ_{br} is given by equation (60). We have from equation (60) (using $\varpi_{\text{acc}} \approx 10^2 \lambda$ and eq. 1)

$$\varpi_{\text{br}} \approx 5 \times 10^8 R_{15}^2 L_{53}^{-1} \left(\frac{\epsilon_{\text{br}}}{4} \right)^{\alpha_2} \text{cm} \approx \frac{5 \times 10^8 R_{15}^2}{40^{\alpha_2} \tau_R^{2\alpha_2/3} L_{53}} \text{cm}. \quad (77)$$

The condition $\varpi_{\text{br}} < \Delta$ reads

$$\frac{\varpi_{\text{br}}}{\Delta} \approx \frac{2 \times 10^{-2} R_{15}^2}{40^{\alpha_2} \tau_R^{2\alpha_2/3} E_{53}} < 1. \quad (78)$$

If the ambient medium is ISM with the optical depth (69) then the condition (78) is not satisfied outside the emission radius of the GRB for any reasonable n_0 and hence the GRB-medium interaction does not produce any break in the GRB spectrum.

If the ambient medium is a wind from a massive progenitor with optical depth (70) then the condition (78) is satisfied at radii $R < R_{\gamma\gamma}$ where

$$R_{\gamma\gamma} \approx 10^{15} \left(\frac{50 E_{53}}{5^{\alpha_2}} \right)^{3/(6+2\alpha_2)} \left(\frac{\dot{M}_{21}}{\mu_e w_8} \right)^{2\alpha_2/(6+2\alpha_2)} \text{cm}. \quad (79)$$

E.g. in the case of $\alpha_2 = 2$ and $\mu_e = 2$ equation (79) yields $R_{\gamma\gamma} \approx 10^{15} E_{53}^{3/10} (\dot{M}_{21}/w_8)^{2/5} \text{cm}$. It can be well outside the emission radius R_{em} and cause a break in the GRB spectrum.

We now derive ϵ_{br} expected in the massive progenitor scenario. We substitute τ_R from equation (70) into equations (76) and (77) and get

$$\epsilon_{\text{br}} \approx 20 R_{15}^{2/3} \left(\frac{\mu_e w_8}{\dot{M}_{21}} \right)^{2/3}. \quad (80)$$

$$\varpi_{\text{br}} \approx 5 \times 10^8 \times 5^{\alpha_2} L_{53}^{-1} R_{15}^{2+2\alpha_2/3} \left(\frac{\mu_e w_8}{\dot{M}_{21}} \right)^{2\alpha_2/3} \text{cm}. \quad (81)$$

The lowest ϵ_{br} is produced at small R in the leading portion of the radiation front $\varpi_{\text{br}} \ll \Delta$. With increasing R , ϖ_{br} and ϵ_{br} grow. A distant observer will see first the leading portion and then deeper layers with increasing ϵ_{br} (the observer's time is

$t_{\text{obs}} = \varpi/c$). Eliminating R from equations (80) and (81) we find

$$\epsilon_{\text{br}}(t_{\text{obs}}) \approx 4 \left(\frac{t_{\text{obs}}}{0.1\text{ms}} L_{53} \right)^{1/(\alpha_2+3)} \left(\frac{\mu_e w_8}{\dot{M}_{21}} \right)^{2/(\alpha_2+3)}. \quad (82)$$

E.g. with $\alpha_2 = 2$ and $\mu_e = 2$ this equation yields $\epsilon_{\text{br}} \approx 30 t_{\text{obs}}^{1/5} L_{53}^{1/5} \dot{M}_{21}^{-2/5} w_8^{2/5}$.

We now see that ϵ_{br} varies across the radiation front as $\epsilon_{\text{br}} \propto \varpi^{1/(\alpha_2+2)}$. This slow variation does not affect strongly the self-similar solution we got in §§ 4 and 5. At $\varpi \sim \varpi_{\text{br}}$ the scattered radiation absorbs almost all the primary photons above the corresponding ϵ_{thr} , causing the break in the spectrum at $\epsilon_{\text{br}} = \epsilon_{\text{thr}}$ and the fall of e^\pm loading (see Fig. 3).

7. EVOLUTION OF THE RADIATION FRONT

In this section we study the front evolution with radius. We start from radius R_{em} where the primary γ -ray pulse is created (possibly by internal shocks in the ejecta, see Piran 1999 for a review). For definiteness one can assume that R_{em} is the radius where the ejecta become transparent,

$$R_{\text{em}} = KR_* \approx 6 \times 10^{13} K L_{53} \Gamma_{\text{ej2}}^{-3} \text{ cm}. \quad (83)$$

Here R_* is the radius of “barion” transparency and $K > 1$ describes a possible increase of the transparency radius owing to pair creation inside the ejecta. Note that $K \gg 1$ would require: (1) a substantial fraction of emitted energy is in γ -rays of energy above the threshold for pair creation, $h\nu \gtrsim \Gamma_{\text{ej}}$ MeV, and (2) the emission is generated at a high rate at radii $R \gg R_*$ (otherwise e^\pm production stops, pairs immediately annihilate down to optical depth ~ 1 and the ejecta become transparent on time-scale R/c because of side expansion). The emission mechanism of GRBs is uncertain and therefore it is unclear whether the two conditions are satisfied. The observed strong variations in many GRBs on time-scales ~ 10 ms indicate that $R_{\text{em}} < 10^{13} \Gamma_{\text{ej2}}^{-2}$ cm in many cases.

The thickness of the radiation pulse is equal to that of the ejecta, $\Delta \approx \Delta_{\text{ej}}$. Radiation is initially collimated within angle $\theta = \Gamma_{\text{ej}}^{-1}$ and moves inside the ejecta. At $R > R_{\text{em}}$ the collimation increases, $\theta = \Gamma_{\text{ej}}^{-1} (R/R_{\text{em}})^{-1}$, and radiation gradually overtakes the ejecta with relative velocity $\approx (1 - \beta_{\text{ej}})c$. The thickness of the radiation pulse emerging ahead of the ejecta and interacting with the ambient medium is growing, $\Delta_i(R) = c(1 - \beta_{\text{ej}})(R/c) = R/2\Gamma_{\text{ej}}^2$. When $\Delta_i(R)$ reaches Δ_{ej} , the whole pulse leaves the ejecta. The corresponding ξ -coordinate of the back boundary of the interacting pulse ξ_Δ is

$$\xi_\Delta(R) = \begin{cases} \frac{\Delta_i}{\lambda} \approx 1.1 \times 10^4 R_{15}^{-1} L_{53} \Gamma_{\text{ej2}}^{-2}, & \frac{R}{2\Gamma_{\text{ej}}^2} < \Delta_{\text{ej}}, \\ \frac{\Delta_{\text{ej}}}{\lambda} \approx 6.5 \times 10^3 R_{15}^{-2} E_{53}, & \frac{R}{2\Gamma_{\text{ej}}^2} > \Delta_{\text{ej}}. \end{cases} \quad (84)$$

7.1. $R_{\text{em}} < R < R_{\text{sat}}$. Saturated surfing

The pulse-medium interaction starts at $R \gtrsim R_{\text{em}}$ with very high $\xi_\Delta \sim 10^6$. The medium entering the pulse accelerates to the equilibrium Lorentz factor

$$\gamma_{\text{sat}}(R) = \Gamma_{\text{ej}} \frac{R}{R_{\text{em}}} \quad (85)$$

at $\xi_c \sim 10^3 \ll \xi_\Delta$ and surfs the pulse. The acceleration time is $\sim (\xi_c \lambda/c) \gamma_{\text{sat}}^2 < R/c$. Note that primary radiation is mixed in the front on scale $\delta\varpi_{\text{mix}} \sim \gamma_{\text{sat}}^{-2} R$ because of the finite angular dispersion $\theta \sim \gamma_{\text{sat}}^{-1}$ of photons. Therefore Lagrangian coordinate ϖ is well defined only on scales $\delta\varpi > \varpi_{\text{mix}}$ (on such scales the radiation can be assumed perfectly collimated with radial velocity c). The ξ -location of the medium in the front is defined with uncertainty $\xi_{\text{mix}} = \varpi_{\text{mix}}/\lambda \sim \xi_\Delta (R/R_{\text{em}})^{-2}$ which exceeds ξ_c at small R where $\xi_c/\xi_\Delta < (R_{\text{em}}/R)^2$.

The equilibrium Lorentz factor $\gamma_{\text{sat}}(R)$ grows with radius. Correspondingly ξ_c [the value of ξ where $\gamma(\xi)$ reaches γ_{sat} , see Fig. 1] grows and reaches $\sim 10^4$ at $R \sim 10^{14}$ cm. At $R = R_{\text{sat}}$,

$$R_{\text{sat}} \approx 1.3 \times 10^{14} \Gamma_{\text{ej2}}^{-3/4} L_{53}^{1/4} R_{\text{em}}^{3/4} \text{ cm}, \quad (86)$$

γ_{sat} exceeds γ_{max} given by equation (29). Then the medium cannot accelerate to γ_{sat} on time R/c and the saturated stage ends.

7.2. $R_{\text{sat}} < R < R_{\text{gap}}$. Unsaturated surfing: caustic

Now ξ_c and γ_c are determined by the condition $(\lambda \xi_c/c) \gamma_c^2 \approx R/c$ (the time of acceleration to γ_c is about R/c). Using equation (62) we get at $\gamma_c > 27$,

$$\frac{\xi_c}{\xi_{\text{acc}}} \approx \frac{53}{\xi_{\text{acc}}^{1/4}} L_{53}^{1/4} R_{15}^{-1/4}, \quad (87)$$

$$\gamma_c \approx \frac{2.0 \times 10^3}{\xi_{\text{acc}}^{3/8}} L_{53}^{3/8} R_{15}^{-3/8}. \quad (88)$$

When R grows from 10^{14} cm to 10^{16} cm, ξ_c decreases slowly from $\xi_c \approx 30 \xi_{\text{acc}}$ to $\xi_c \approx 10 \xi_{\text{acc}}$. Correspondingly, γ_c decreases from $\approx 10^3$ to ≈ 140 . Hereafter we substitute in all estimates $\xi_{\text{acc}} = 120$ keeping in mind the typical $\alpha_2 = 1.5$; for $\alpha_2 = 2$ there is a slight change $\xi_{\text{acc}} = 150$ (see § 5.2).

The new material trapped at given R comes to ξ_c with smaller γ compared to that of the already accumulated material in the front. This results in “overshooting” and implies appearance of a caustic. The overshooting can be seen e.g. in the ϖ -coordinate: the accumulated material has $\varpi_c^{\text{old}} = \xi_c \lambda$ and the newly trapped material comes to $\varpi_c^{\text{new}} = R/\gamma_c$. Hence, $\varpi_c^{\text{new}}/\varpi_c^{\text{old}} \propto \xi_c/\gamma_c$. With decreasing ξ_c , the condition for overshooting reads $d(\xi/\gamma)/d\xi < 0$ at $\xi = \xi_c$, or

$$\left[\frac{d \ln \gamma}{d \ln \xi} \right]_{\xi=\xi_c} > 1, \quad (89)$$

which is satisfied in the range of interest $\xi \sim 10^3 - 10^4$. The caustic results in a shock. If the shock is radiative (which is likely the case since the material is pair-dominated and the Compton cooling is very efficient) then the shocked matter piles up in a thin shell.

When the caustic appears, the accumulated ion material starts to decelerate and the e^\pm stream behind ξ_c hits the ion medium. One can show that the momentum of the e^\pm stream exceeds by a factor ~ 10 the momentum of the accumulated ions and this “reverse” shock should be strong. For simplicity, we will neglect the impact of the e^\pm stream on the surfing medium (inclusion of this effect will slightly increase the radius R_{gap} derived below).

The medium surfs the pulse with $\gamma \approx \gamma_c$ until ξ_Δ reaches ξ_c . This happens at some radius R_c . At $R > R_c$ the whole front

$0 < \xi < \xi_\Delta$ is described by the self-similar solution. We now consider two possible cases.

1. $R_c < 2\Gamma_{\text{ej}}^2 \Delta_{\text{ej}}$. — The ejecta catch up with the surfing medium before the whole γ -ray pulse leaves the ejecta. Then $\xi_c = \xi_\Delta$ gives (using eqs. 84 and 87)

$$R_c = \frac{1.2 \times 10^{18}}{\xi_{\text{acc}}} \frac{L_{53}}{\Gamma_{\text{ej}2}^{8/3}} \text{ cm} \approx 10^{16} \frac{L_{53}}{\Gamma_{\text{ej}2}^{8/3}} \text{ cm}. \quad (90)$$

At $R = R_c$ we also have $\gamma_c \approx \Gamma_{\text{ej}}$ i.e. the ejecta touch the medium with a small relative Lorentz factor and start to decelerate. The gap between the surfing medium and the ejecta disappears at this moment; we thus have $R_{\text{gap}} = R_c$.

The condition $R_c < 2\Gamma_{\text{ej}}^2 \Delta_{\text{ej}}$ requires

$$t_b > \frac{45}{\xi_{\text{acc}}^{1/2}} \frac{E_{53}^{1/2}}{\Gamma_{\text{ej}2}^{7/3}} \text{ s} \approx 4 \frac{E_{53}^{1/2}}{\Gamma_{\text{ej}2}^{7/3}} \text{ s}, \quad (91)$$

where we used $t_b = \Delta_{\text{ej}}/c = E/L$. This condition implies

$$R_{\text{gap}} = R_c < \frac{3 \times 10^{16}}{\xi_{\text{acc}}^{1/2}} \frac{E_{53}^{1/2}}{\Gamma_{\text{ej}2}^{1/3}} \text{ cm} \approx 3 \times 10^{15} \frac{E_{53}^{1/2}}{\Gamma_{\text{ej}2}^{1/3}} \text{ cm}. \quad (92)$$

2. $R_c > 2\Gamma_{\text{ej}}^2 \Delta_{\text{ej}}$. — The whole γ -ray pulse leaves the ejecta before they reach R_c . Then equation $\xi_c = \xi_\Delta$ gives

$$R_c = \frac{1.6 \times 10^{16}}{\xi_{\text{acc}}^{3/7}} E_{53}^{3/7} t_b^{1/7} \text{ cm} \approx 2 \times 10^{15} E_{53}^{3/7} t_b^{1/7} \text{ cm}. \quad (93)$$

The value of $\gamma_c(R_c)$ now differs from Γ_{ej} ,

$$\gamma_c = \frac{7.1 \times 10^2}{\xi_{\text{acc}}^{3/14}} E_{53}^{3/14} t_b^{-3/7}. \quad (94)$$

The condition $R_c > 2\Gamma_{\text{ej}}^2 \Delta_{\text{ej}}$ (which is equivalent to the inequality opposite to 91) implies that $\gamma_c > \Gamma_{\text{ej}}$ and hence the gap still exists after $R = R_c$. The gap disappears when $\gamma(\xi_\Delta) \approx \Gamma_{\text{ej}}$ (then the ejecta catch up with the surfing medium). This condition yields

$$R_{\text{gap}} = \frac{3 \times 10^{16}}{\xi_{\text{acc}}^{1/2}} \frac{E_{53}^{1/2}}{\Gamma_{\text{ej}2}^{1/3}} \text{ cm} \approx 3 \times 10^{15} \frac{E_{53}^{1/2}}{\Gamma_{\text{ej}2}^{1/3}} \text{ cm}. \quad (95)$$

7.3. $R_{\text{gap}} < R < R_{\text{acc}}$. Preaccelerated pair-rich medium

In this range of radii ξ_Δ decreases from $\xi_c(R_{\text{gap}})$ to $\xi_{\text{acc}} \approx 10^2$. Correspondingly $\gamma(\xi_\Delta)$ decreases from Γ_{ej} to ≈ 1 . When ξ_Δ reaches ξ_{acc} the medium cannot be relativistically accelerated anymore. This happens at radius

$$R_{\text{acc}} = \frac{R_\lambda}{\xi_{\text{acc}}^{1/2}} \approx 7 \times 10^{15} E_{53}^{1/2} \text{ cm}, \quad (96)$$

where R_λ is given by equation (2).

7.4. $R_{\text{acc}} < R < R_{\text{load}}$. Non-relativistic pair-rich medium

At $R > R_{\text{acc}}$ the radiation front still loads the medium with a large number of pairs. At $R = R_{\text{acc}}$ ($\xi_\Delta = \xi_{\text{acc}}$) we have $n^*/n_0 \approx 75$ behind the front and with increasing R the pair

loading decreases exponentially (see eq. 49). The pair loading ends at $R = R_{\text{load}}$ (ξ_Δ reaches ξ_{load} and $n^*/n_0 \sim 1$),

$$R_{\text{load}} = \frac{R_\lambda}{\xi_{\text{load}}^{1/2}} \approx 1.6 \times 10^{16} E_{53}^{1/2} \text{ cm}. \quad (97)$$

In § 5 we showed that ξ_{acc} is related to ξ_{load} by a simple formula $\xi_{\text{acc}} = (5 + \ln \mu_e) \xi_{\text{load}}$ which weakly depends on μ_e ($1 < \mu_e < 2$). Hence, we have a relation

$$R_{\text{load}} = (5 + \ln \mu_e)^{1/2} R_{\text{acc}} = (2.3 \pm 0.1) R_{\text{acc}}. \quad (98)$$

7.5. $R > R_{\text{load}}$. Front weakly affects the medium

Here $\xi_\Delta < \xi_{\text{load}}$ and both e^\pm loading and acceleration are shut down. The blast wave sweeps the normal pair-free static medium.

8. BLAST WAVE

8.1. Dynamics

We will model the blast wave in a simplified way, as a thin shell sweeping the ambient medium. This is a good approximation to the exact hydrodynamic solution with forward and reverse shocks if the ejected shell is sufficiently thin, so that the reverse shock crosses Δ_{ej} on time less than R/c (e.g. Piran 1999).

The shell has initial mass M_{ej} and Lorentz factor Γ_{ej} and starts to sweep the ambient medium at $R = R_{\text{gap}}$ (see § 7). At a radius $R > R_{\text{gap}}$ the shell has mass $M > M_{\text{ej}}$ and Lorentz factor $\Gamma < \Gamma_{\text{ej}}$. When it sweeps mass element dm that moves with Lorentz factor γ , Γ decreases by $d\Gamma$ and energy dE_{diss} is dissipated. The laws of energy and momentum conservation read

$$\Gamma M + \gamma dm = (\Gamma + d\Gamma)(M + dm + dm_{\text{heat}}), \quad (99)$$

$$\Gamma \hat{\beta} M + \gamma \beta dm = (\Gamma + d\Gamma)(\hat{\beta} + d\hat{\beta}) \times (M + dm + dm_{\text{heat}}). \quad (100)$$

Here $\hat{\beta} = (1 - 1/\Gamma^2)^{1/2}$ and $dm_{\text{heat}} = (dE_{\text{diss}}/c^2 \Gamma)$ is the rest mass associated with the dissipated heat. The inertial mass M includes the initial mass of the ejecta M_{ej} , the swept mass $m(R)$, and the stored heat. Assuming that a fraction η of heat is radiated away, one gets the dynamic equations

$$M \frac{d\Gamma}{dm} = \Gamma^2 \hat{\beta} \gamma (\beta - \hat{\beta}), \quad (101)$$

$$\frac{dM}{dm} = \eta + (1 - \eta) \Gamma \gamma (1 - \hat{\beta} \beta). \quad (102)$$

The radiated energy is

$$\frac{dE_{\text{rad}}}{dm} = \eta \frac{dE_{\text{diss}}}{dm} = \eta c^2 \Gamma [\Gamma \gamma (1 - \hat{\beta} \beta) - 1]. \quad (103)$$

The swept mass is related to radius by $dm/dR = 4\pi R^2 \rho_0$ where $\rho_0(R)$ is the density of the (static) medium ahead of the radiation front. The front affects the blast wave dynamics by increasing γ of the medium just before it is swept by the blast wave. Note that there is no substantial increase of the medium mass by e^\pm loading in the front at $R > R_{\text{gap}}$ (see § 7). The dynamic equations acquire the standard form if $\gamma = 1$ (deceleration by static medium, see Piran 1999).

Radiative preacceleration and subsequent sweeping by the ejecta shell are separated by a small interval of time ($\ll R/c$), so that preacceleration can be treated locally at a given R . Indeed, the distance between the leading boundary of the radiation front and the blast wave is $\Delta_f \approx R/2\Gamma^2$ (the front velocity is taken equal to c in this estimate). The sweeping time is $t_{\text{sw}} = (\Delta_f/c)2\gamma^2 = (R/c)(\gamma/\Gamma)^2 \ll R/c$ at any $R > R_{\text{gap}}$. The medium Lorentz factor ahead of the blast wave is that behind the radiation front, $\gamma = \gamma(\xi_\Delta)$. For a given R , $\gamma(\xi_\Delta)$ is found from the front solution (§§ 4 and 5) where one should substitute

$$\xi_\Delta = \left(\frac{R_\lambda}{R} \right)^2 = \frac{\xi_{\text{acc}}}{x^2}, \quad x \equiv \frac{R}{R_{\text{acc}}}. \quad (104)$$

We will use the analytical formula (62) which is a good approximation to the exact solution. Then we have

$$\gamma(x) = \begin{cases} 1, & x > 1, \\ x^{-6}, & \frac{1}{\sqrt{3}} < x < 1, \\ 3\sqrt{3}x^{-3}, & x_{\text{gap}} < x < \frac{1}{\sqrt{3}}. \end{cases} \quad (105)$$

Here $x_{\text{gap}} = R_{\text{gap}}/R_{\text{acc}} \approx 0.3$ is the radius where $\gamma = \Gamma_{\text{ej}}$ and the ejecta start to sweep the ambient medium.

The characteristic mass of the problem is the ambient mass within the acceleration radius,

$$m_{\text{acc}} = \int_0^{R_{\text{acc}}} 4\pi R^2 \rho_0 dR. \quad (106)$$

The mass swept before the blast wave reaches a radius $x = R/R_{\text{acc}}$ is

$$m(x) = m_{\text{acc}} x^k. \quad (107)$$

Here k characterizes the radial distribution of the ambient density ρ_0 . E.g. $k = 3$ for constant density medium and $k = 1$ for a wind with constant \dot{M} and w .

As long as the dissipated energy $E_{\text{diss}} \ll E_{\text{ej}} = \Gamma_{\text{ej}} M_{\text{ej}} c^2$ (and $\Gamma \approx \Gamma_{\text{ej}}$) we have from equation (103) $dE_{\text{diss}}/dm \approx \Gamma_{\text{ej}}^2 c^2 \gamma^{-1} (1 + \beta)$ (at $\gamma \ll \Gamma_{\text{ej}}$). Replacing the varying factor $1 + \beta$ by unity, we get an estimate

$$E_{\text{diss}}(x) \approx \Gamma_{\text{ej}}^2 m_{\text{acc}} c^2 \begin{cases} x^k - \frac{6}{k+6}, & x > 1, \\ \frac{kx^{k+6}}{k+6}, & \frac{1}{\sqrt{3}} < x < 1. \end{cases} \quad (108)$$

Here we neglected the small energy dissipated at $x < 1/\sqrt{3}$. Equation (108) assumes a deceleration radius $x_{\text{dec}} > 1$. Setting $E_{\text{diss}} = E_{\text{ej}}$ we find the actual deceleration radius,

$$x_{\text{dec}} \approx \begin{cases} \left[\frac{6}{k+6} (1 + \frac{1}{D}) \right]^{1/k}, & \text{if } x_{\text{dec}} > 1, \\ D^{-1/(k+6)}, & \text{if } \frac{1}{\sqrt{3}} < x_{\text{dec}} < 1, \end{cases} \quad (109)$$

where

$$D \equiv \frac{k \Gamma_{\text{ej}}^2 m_{\text{acc}} c^2}{(k+6) E_{\text{ej}}}. \quad (110)$$

In the regime $D \ll 1$ ($x_{\text{dec}} \gg 1$) equation (109) yields

$$x_{\text{dec}}^k = \frac{6E_{\text{ej}}}{k\Gamma_{\text{ej}}^2 m_{\text{acc}} c^2}, \quad m(x_{\text{dec}}) = \frac{6E_{\text{ej}}}{k\Gamma_{\text{ej}}^2 c^2}. \quad (111)$$

This gives the standard estimate for R_{dec} equivalent to the condition that the swept mass is about $E_{\text{ej}}/\Gamma_{\text{ej}}^2 c^2$ (e.g. Rees & Mészáros 1992).

In the regime $D > 1$ deceleration occurs in the relativistically moving medium. In this case the mass swept at x_{dec} is $\sim (E_{\text{ej}}/\Gamma_{\text{ej}}^2 c^2) \gamma(x_{\text{dec}})$ where $\gamma(x_{\text{dec}})$ is found from equations (105) and (109),

$$\gamma(x_{\text{dec}}) = \begin{cases} 1, & x_{\text{dec}} > 1, \\ D^{6/(k+6)}, & \frac{1}{\sqrt{3}} < x_{\text{dec}} < 1. \end{cases} \quad (112)$$

The deceleration radius remains close to R_{acc} even at $D \gg 1$. (Note that the parameter D is limited from above by the transparency condition 72).

If the ambient medium is ISM with constant density $n_0 \sim 1 \text{ cm}^{-3}$ we have $k = 3$ and $m_{\text{acc}} = 2.4 \times 10^{24} \mu_e n_0 E_{53}^{3/2} \text{ g}$. The parameter D is then given by

$$D = 7.3 \times 10^{-5} \mu_e n_0 E_{53}^{3/2} E_{\text{ej}53}^{-1} \Gamma_{\text{ej}2}^2. \quad (113)$$

Hence the deceleration radius is in the static region $x_{\text{dec}} > 1$ if $n_0 < 10^4 \Gamma_{\text{ej}2}^{-2} E_{\text{ej}53} E_{53}^{-3/2} \text{ cm}^{-3}$. The standard estimate $R_{\text{dec}} \sim (3E_{\text{ej}}/4\pi\Gamma_{\text{ej}}^2 \rho_0 c^2)^{1/3}$ then applies. Equation (108) (with $k = 3$) yields the energy fraction that is dissipated at $x < 1$, $f_{\text{acc}} \approx (1/3)x_{\text{dec}}^{-3}$. The fraction dissipated in the static pair-loaded zone, $1 < x < x_{\text{load}} \approx 2.3$ (eq. 98), is $f_{\text{load}} \approx (x_{\text{load}}/x_{\text{dec}})^3 \approx 20D$. For typical parameters $f_{\text{load}} < 1\%$.

In the massive progenitor scenario (e.g. Woosley 1993, Chevalier & Li 1999) the ambient medium of the GRB is a wind from the progenitor. From a Wolf-Rayet progenitor one expects a wind with mass loss $\dot{M} \sim 10^{-5} M_\odot \text{ yr}^{-1}$ and velocity $w \sim 10^3 \text{ km s}^{-1}$ (Chevalier & Li 1999). In the case of a red giant progenitor, the wind velocity is smaller, $w \sim 10 \text{ km s}^{-1}$, and then the ambient density is higher. The wind medium is described by $k = 1$ and $m_{\text{acc}} = (\dot{M}/w)R_{\text{acc}} = 7 \times 10^{28} \dot{M}_{21} w_8^{-1} E_{53}^{1/2} \text{ g}$. The parameter D is then given by

$$D = \frac{\dot{M} c^2 \Gamma_{\text{ej}}^2}{7w E_{\text{ej}}} R_{\text{acc}} \approx \dot{M}_{21} w_8^{-1} E_{53}^{1/2} E_{\text{ej}53}^{-1} \Gamma_{\text{ej}2}^2. \quad (114)$$

The typical D is comparable or much larger than unity and the effects of the medium preacceleration by the radiation front must affect strongly the blast wave dynamics.

To study the wind case in more detail we solve numerically equations (101, 102, 105, 107). Figure 4 shows the results for $\Gamma_{\text{ej}} = 200$, $E = E_{\text{ej}} = 10^{53} \text{ erg}$ (the energy of the gamma-ray pulse is equal to that of the ejecta), and $\eta = 1$. The chosen values of $\dot{M}/w = 2.5 \times 10^{-5}$, 2.5×10^{-3} , 0.25, and 12.5, correspond to $D = 10^{-4}$, 10^{-2} , 1, and 50, respectively. In the regime $D \geq 1$ one can see the strong peak of energy dissipation at $x \sim 1$. In the case of $D = 50$, 80% of the blast wave energy is dissipated at $0.5 < x < 1$ and 99% at $0.3 < x < 2$.

8.2. Emission

We now evaluate the main characteristics of the blast wave emission, in particular, the bolometric light curve seen by a distant observer and the peak synchrotron frequency. A detailed analysis is deferred to a next paper.

8.2.1. Bolometric light curve

A distant observer will see a mixture of radiation emitted by the shell at different radii. Denote the arrival time of radiation by t_{obs} and choose $t_{\text{obs}} = 0$ for a light signal that would come from the center/beginning of the explosion. First consider the observed light curve from instantaneous emission of energy E_0 by the shell at radius R . The shell reaches this radius at time $t(R)$ after the beginning of the explosion. Choose a polar axis pointing towards the observer. The observer will first receive photons emitted at $\theta = 0$ ($\mu = \cos \theta = 1$). These first photons come at $t_{\text{obs}} = t(R) - R/c$ and photons emitted from a circle $\mu = \text{const} < 1$ will arrive with a delay of $(R/c)(1 - \mu)$. We thus have a relation

$$t_{\text{obs}}(R, \mu) = t(R) - \frac{R}{c}\mu, \quad t(R) = \int_0^R \frac{dR}{\hat{\beta}c}. \quad (115)$$

Radiation received at δt_{obs} comes from the ring $|\delta\mu| = \delta t_{\text{obs}}(c/R)$. The total energy emitted by this ring (in all directions) equals $\delta E = E_0|\delta\mu|/2$ where $|\delta\mu|/2$ is the fraction of the shell surface occupied by the ring. We will assume that each element of the ring emits isotropically in its rest frame. Radiation emitted towards the observer within a solid angle $d\tilde{\Omega}$ in the rest frame occupies $d\Omega = \Gamma^2(1 - \hat{\beta}\mu)^2 d\tilde{\Omega}$ in the lab frame. Hence the observed flux is affected by the beaming factor $\Gamma^{-2}(1 - \hat{\beta}\mu)^{-2}$ and the *apparent* isotropic energy seen by the observer from a ring $\delta\mu$ is $\delta E_{\text{app}} = \Gamma^{-2}(1 - \hat{\beta}\mu)^{-2}\delta E$. (Integration of δE_{app} over the shell gives E_0 as it should be.) The apparent isotropic luminosity is

$$L_{\text{obs}} = \frac{\delta E_{\text{app}}}{\delta t_{\text{obs}}} = \frac{cE_0}{2\Gamma^2 R} \left\{ 1 - \frac{\hat{\beta}c}{R} [t(R) - t_{\text{obs}}] \right\}^{-2}. \quad (116)$$

From the dynamic solution we know dE_{diss}/dR and $\Gamma(R)$. It allows us to compute the observed light curve from the whole history of the shell deceleration (we substitute $E_0 = [dE_{\text{diss}}/dR]dR$ into eq. 116 and integrate over R),

$$L_{\text{obs}}(t_{\text{obs}}) = \int_0^{R_{\text{max}}(t_{\text{obs}})} \frac{(R/c)(dE_{\text{diss}}/dR)dR}{2\Gamma^2[R/c - \hat{\beta}(t - t_{\text{obs}})]^2}, \quad (117)$$

where $R_{\text{max}}(t_{\text{obs}})$ is defined by condition $t(R) - R/c = t_{\text{obs}}$ (see eq. 115).

The results are shown in Figure 5 for the blast waves in wind environment with $D = 10^{-4}, 10^{-2}, 1$, and 50 (same cases as in Fig. 4). There is no emission until $t_{\text{rise}} = R_{\text{gap}}/2\Gamma_{\text{ej}}^2 \approx E_{53}^{1/2}(\Gamma_{\text{ej}}/200)^{-7/3}$ s which corresponds to the moment when the ejecta catch up with the surfing medium and start to decelerate. At $t_{\text{obs}} = t_{\text{rise}}$ the light curve rises steeply and then reaches a peak at

$$t_{\text{peak}} \approx \frac{R_{\text{acc}}}{2\Gamma_{\text{ej}}^2} \left\{ \begin{array}{ll} 1, & D < 1 \\ x_{\text{dec}}, & D > 1 \end{array} \right\} \approx 12 \frac{E_{53}^{1/2}}{\Gamma_{\text{ej}}^2} \text{ s}. \quad (118)$$

Since x_{dec} remains close to unity even at $D \gg 1$, we get a universal t_{peak} in a very wide range of D . In the examples shown in Figure 5 ($E_{53} = 1, \Gamma_{\text{ej}} = 2$) we get $t_{\text{peak}} \sim 3$ s. At $D < 10^{-2}$ there appears a plateau in the light curve between t_{peak} and $\sim 0.1R_{\text{dec}}/2\Gamma_{\text{ej}}^2 c$.

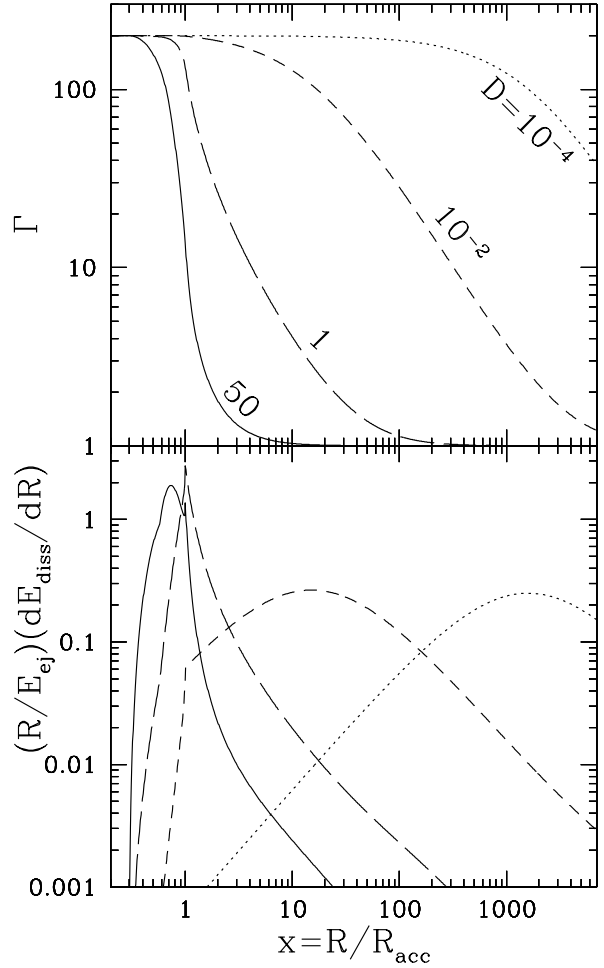


FIG. 4.— Blast wave dynamics in a wind. Here $E = E_{\text{ej}} = 10^{53}$ erg, $\Gamma_{\text{ej}} = 200$, $\eta = 1$. Dotted, dashed, long-dashed, solid curves display the cases $D = 10^{-4}, 10^{-2}, 1, 50$ (see eq. 114).

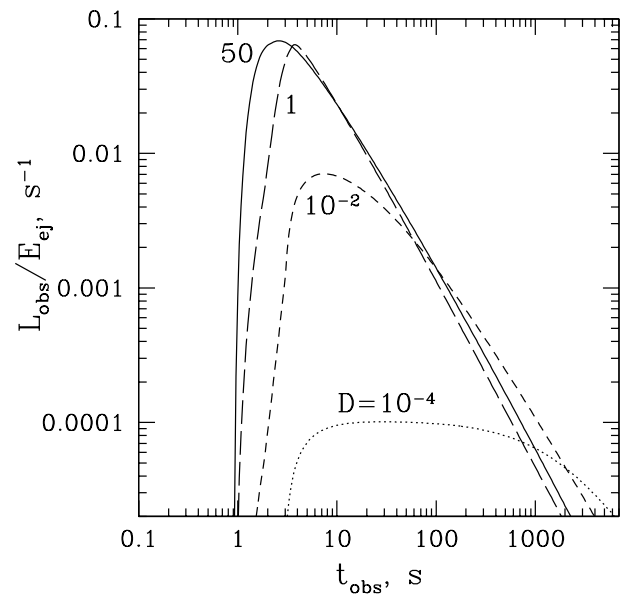


FIG. 5.— Bolometric light curves from the blast waves shown in Figure 4.

8.2.2. Synchrotron peak frequency

The medium encountered by the blast wave is e^\pm -loaded, preaccelerated, and compressed by the radiation front. Correspondingly, the standard analysis of the blast wave emission (Blandford & McKee 1977; Piran 1999) applies to our case with three modifications: (1) e^\pm loading increases the number of shocked electrons by the factor n^*/n_0 . (2) The proper mass density of the medium is $\tilde{\rho} = \rho_0 \gamma^{-1} (1 - \beta)$ rather than ρ_0 ; here the factor $(1 - \beta)$ comes from compression in the front (cf. § 3.2) and γ^{-1} appears due to Lorentz stretching when we go to the rest frame. (3) The medium Lorentz factor in the shock frame is $\sim \Gamma/\gamma$ rather than Γ .

The proper energy density of the postshock material is

$$u = 4(\Gamma/\gamma)^2 \tilde{\rho} c^2. \quad (119)$$

Assuming that the magnetic energy $B^2/8\pi$ is a fraction ϵ_B of u , we have

$$B = c \frac{\Gamma}{\gamma} \sqrt{\frac{32\pi\epsilon_B\rho_0}{\gamma(1-\beta)}}. \quad (120)$$

Assuming that e^\pm share the energy of shocked ions, the mean randomized Lorentz factor of e^\pm in the rest-frame of shocked matter is

$$\gamma_e = \mu_e \frac{m_p}{m_e} \frac{\Gamma}{\gamma} \frac{n_0}{n^*}, \quad (121)$$

where $1 < \mu_e < 2$ (see eq. 13).

We then get the peak synchrotron frequency in the rest-frame,

$$\tilde{\nu}_s \approx 10^6 B \gamma_e^2 \text{ Hz} \approx \frac{10^{30} \rho_0^{1/2}}{\gamma^{5/2}} \left(\frac{n_0}{n^*} \right)^2 \mu_e^2 \epsilon_B^{1/2} \Gamma^3 \text{ Hz}. \quad (122)$$

The corresponding observed frequency is $\nu_s = \tilde{\nu}_s \Gamma(1+z)^{-1}$ where z is the redshift of the burst.

For example consider a blast wave with $D \ll 1$ in ISM. At radii $R_{\text{acc}} < R < R_{\text{dec}}$ we have $\Gamma \approx \Gamma_{\text{ej}}$ and $\gamma \approx 1$. The density n^* is given by equation (49) with $\varpi/a = (R_{\text{load}}/R)^2$. Then from equation (122) we get

$$\tilde{\nu}_s \approx \frac{4 \times 10^{18} \mu_e^2 \epsilon_B^{1/2} n_0^{1/2} \Gamma_{\text{ej}}^3}{\exp(2R_{\text{load}}^2/R^2) + \exp(-2R_{\text{load}}^2/R^2) + 2} \text{ Hz}, \quad (123)$$

$$R_{\text{acc}} < R < R_{\text{load}}.$$

For instance, the observed emission from $R = R_{\text{acc}}$ has the peak frequency $\nu_s \approx 8 \times 10^{16} (1+z)^{-1} \mu_e^2 \epsilon_B^{1/2} n_0^{1/2} \Gamma_{\text{ej}}^4$ Hz. The emission from $R < R_{\text{acc}}$ is even softer, however, the luminosity is small from that region (see eq. 108).

As a second example, consider a blast wave in a wind with $D > 1$ and evaluate the peak frequency at the deceleration radius $R_{\text{dec}} < R_{\text{acc}}$. Substituting equations (109,112) into equation (123) and using (63) we get

$$\tilde{\nu}_s \approx \frac{4 \times 10^{16}}{D^3} \Gamma_{\text{ej}}^3 \epsilon_B^{1/2} \left(\frac{\dot{M}_{21}}{\mu_e w_8} \right)^{1/2} \text{ Hz}. \quad (124)$$

E.g. for $D = 20$, $\Gamma_{\text{ej}} = 10^2$, and $\epsilon_B \sim 1$, the observed $\nu_s = \tilde{\nu}_s \Gamma(1+z)^{-1}$ is in the optical and hence a large fraction of the blast wave energy is emitted in the optical band.

9. CONCLUSIONS

The unusual character of radiation fronts in GRBs is owing to two basic facts: (1) the front is opaque for scattered radiation ($\gamma - \gamma$ opacity) and (2) the front is “opaque” for ambient electrons – the electron scatters many times when passing through the front. The first property causes e^\pm loading and the second – violent acceleration of the medium. The processes occurring in the radiation front are crucially important since they “prepare” the medium encountered by the blast wave. We summarize the main features of the medium dynamics in the front in § 9.1 and its impact on the blast wave in § 9.2. The front should cause spectacular observational effects during the early afterglow, possibly overlapping with the prompt GRB. The expected phenomena are briefly discussed in § 9.3.

9.1. The radiation front

1. The medium is heated in the process of pair loading. However, Compton cooling keeps the bulk of particles at modest (non-relativistic) energies throughout the front.
2. Photons scattered at one portion of the front get absorbed at a different portion far behind the location of scattering. The local approximation assuming that the scattered photons instantaneously become e^\pm is not adequate: the front structure is governed by the non-local processes. Yet a simple analytical description can be given to this non-local structure (§ 5).
3. At sufficiently large radii ($R > R_c$, see § 7) the whole front has a quasi-steady structure established on time-scales $\ll R/c$. The front is described by a self-similar solution $n(\xi)$, $\gamma(\xi)$ where $\xi = \varpi/\lambda \propto R^{-2}$. Here $0 < \varpi < \Delta$ measures distance inside the front ($\varpi = 0$ at the leading boundary), and $\lambda \propto R^2$ is the electron free-path in the radiation field (eq. 1). In the leading portion of the front the medium density exponentiates due to pair loading on length $\xi_{\text{load}} \approx 30$, at $\xi_{\text{acc}} \approx 5\xi_{\text{load}}$ the medium starts to accelerate relativistically, and at $\xi_{\pm} \approx 30\xi_{\text{load}}$ the loaded pairs outnumber the ambient protons by the factor m_p/m_e and dominate the inertia of the medium. The medium parameters behind the front are $n(\xi_\Delta)$ and $\gamma(\xi_\Delta)$ where $\xi_\Delta = \Delta/\lambda \propto R^{-2}$ is the trailing boundary of the front. The radius of the relativistically preaccelerated region is found from the condition $\xi_\Delta = \xi_{\text{acc}}$ which gives $R_{\text{acc}} = 7 \times 10^{15} E_{53}^{1/2}$ cm. At $R > R_{\text{acc}}$ the front still loads the medium with e^\pm . At $R > R_{\text{load}} = 1.5 \times 10^{16} E_{53}^{1/2}$ cm the e^\pm loading is shut down ($\xi_\Delta < \xi_{\text{load}}$).
4. At small $R < R_c \sim R_{\text{acc}}/4$ the medium is accelerated so strongly that it gets “stuck” in the radiation front (the time-scale for the medium dynamics across Δ exceeds R/c). Then two zones exist in the front: (1) $\xi < \xi_c \sim 10^3 - 10^4$ – here the steady self-similar structure is established and (2) $\xi > \xi_c$ – the ion-free zone. Being strongly accelerated, the ambient medium cannot penetrate the zone $\xi_c < \xi < \xi_\Delta$. Instead, it accumulates at $\xi \sim \xi_c$ and surfs the radiation pulse. With increasing R the front traps new material which is accelerated to a smaller velocity. It causes the overshooting effect and a caustic appears in the surfing medium (§ 7.2).

The surfing stage is finished at the radius R_c which is equal or smaller than the radius of the blast wave formation (see § 7.2). At the blast-wave stage the whole radiation front is described by the self-similar solution $\gamma(\xi)$, $n(\xi)$. The front leaves behind the accelerated and e^\pm -loaded material which is then swept by the blast wave.

9.2. The blast wave

1. The blast wave forms at $R = R_{\text{gap}}$. For short bursts ($t_b < 4E_{53}^{1/2}\Gamma_{\text{ej2}}^{-7/3}$ s) $R_{\text{gap}} \approx 3 \times 10^{15} E_{53}^{1/2}\Gamma_{\text{ej2}}^{-1/3}$ cm. For longer bursts $R_{\text{gap}} \approx 10^{16} t_b^{-1} E_{53}\Gamma_{\text{ej2}}^{-8/3}$ cm.
2. In a constant density medium, the blast wave decelerates in the region $R_{\text{dec}} > R_{\text{acc}}$ if the ambient density $n_0 < 10^4 \Gamma_{\text{ej2}}^{-2} E_{53} E_{53}^{-3/2}$ cm $^{-3}$. Such conditions probably take place for explosions in ISM.
3. If the explosion happens in a wind from a massive progenitor the radiation front affects strongly the blast wave deceleration. We defined a parameter D (eq. 114) that controls the dynamics and showed that the blast wave is likely in the regime $D > 1$ which corresponds to $R_{\text{dec}} < R_{\text{acc}}$, i.e. deceleration occurs in relativistically moving medium. The standard estimate of R_{dec} is then invalid, and instead one should use the formula (109). The blast wave decelerates close to the unique radius $R_{\text{acc}} \approx 7 \times 10^{15} E_{53}^{1/2}$ cm and R_{dec} weakly depends on the medium parameters as long as $D > 1$. Roughly speaking, the blast wave does not decelerate until it approaches R_{acc} and then violent deceleration occurs: $\sim 90\%$ of the ejecta energy can be dissipated at $R \sim R_{\text{acc}}$.

The strong effect of the radiation front on the blast wave formation and dynamics can be easily understood. The front passes energy $\delta E \sim \delta\tau E$ to ambient mass δm ahead of the ejecta, where $\delta\tau \sim 0.2\sigma_T\delta m(4\pi R^2 m_*)^{-1}$ is the optical depth of δm (here 0.2 is a Klein-Nishina correction and m_* is mass per electron, $m_* < m_p$ due to pair loading). The Lorentz factor of the accelerated medium is

$$\gamma - 1 = \frac{\delta E}{c^2 \delta m} = \frac{\delta\tau}{\delta m} \frac{E}{c^2} = \frac{0.2\sigma_T}{4\pi R^2 m_*} \frac{E}{c^2}. \quad (125)$$

The front structure solution gives m_* and γ behind the front; e.g. $m_* \approx m_p/75$ at $R = R_{\text{acc}}$. At even smaller radii $R < R_{\text{gap}} \sim R_{\text{acc}}/3$, $\gamma > \Gamma_{\text{ej}}$ – the accelerated medium runs away from the ejecta (the gap is opened).

The blast wave starts to decelerate when the swept inertial mass measured in the ejecta rest frame ($\Gamma_{\text{ej}}/\gamma$) $m \sim M_{\text{ej}}$ [here $m(R)$ is the swept rest mass]. The deceleration radius is strongly affected by the medium preacceleration despite the fact that only small energy $e \ll E_{\text{ej}} = \Gamma_{\text{ej}} M_{\text{ej}} c^2$ was used to accelerate the medium. Indeed, we have

$$m(R_{\text{dec}}) \sim \frac{M_{\text{ej}}}{\Gamma_{\text{ej}}} \gamma(R_{\text{dec}}), \quad e = (\gamma - 1)m \sim E_{\text{ej}} \frac{\gamma(\gamma - 1)}{\Gamma_{\text{ej}}^2}. \quad (126)$$

With increasing γ , R_{dec} grows markedly [$m(R_{\text{dec}}) \propto \gamma(R_{\text{dec}})$] while the energy e used for the medium preacceleration remains much smaller than E_{ej} since $\gamma(R_{\text{dec}}) < \Gamma_{\text{ej}}$.

9.3. Expected observational phenomena

1. The generic prediction is that the early emission of a GRB blast wave (at $t_{\text{obs}} < 30E_{53}^{1/2}\Gamma_{\text{ej2}}^{-2}$ s) should be very soft. Compared to the standard model that neglects the effects of the radiation front, the peak frequency of synchrotron emission is reduced by the pair loading factor $(m_*/m_p)^2 = (n^*/n_0)^{-2}$ and the preacceleration factor $\gamma^{-5/2}$ (see eq. 122). The early afterglow (possibly overlapping with the prompt GRB) should start as a relatively weak optical signal at $R < R_{\text{acc}}$ and then the peak frequency moves to the X-ray band; at $R > R_{\text{load}}$ the blast wave sweeps the normal e^\pm -free static medium and emits in the standard regime.
2. The fraction f of the afterglow energy that is emitted at the early soft stage is controlled by the ratio $R_{\text{load}}/R_{\text{dec}}$. In the typical ISM environment $f < 1\%$. In the typical wind environment with $D > 1$ (eq. 114), most of the blast wave energy is emitted at the early soft stage. The violent deceleration that happens at $R \sim R_{\text{acc}}$ should cause a strong peak in the soft light curve.
3. The expected soft light curves from blast waves in winds have special features that are easy to recognize in observations. E.g. in the short burst regime ($t_b < 4E_{53}^{1/2}\Gamma_{\text{ej2}}^{-7/3}$ s) one expects (1) a steep rise at $t_{\text{rise}} \approx R_{\text{gap}}/2\Gamma_{\text{ej}}^2 \approx E_{53}^{1/2}\Gamma_{\text{ej2}}^{-2}$ and (2) a peak at $t_{\text{peak}} \approx (R_{\text{acc}}/R_{\text{gap}})t_{\text{rise}} \approx 2.3\Gamma_{\text{ej2}}^{1/3}t_{\text{rise}}$. Both t_{rise} and t_{peak} depend weakly on the wind parameters in a wide range $10^{-3} < D < 10^2$ (§ 8.2.1). Given the observed E and t_{peak} one can find the Lorentz factor of the ejecta. If Γ_{ej} does not vary strongly from burst to burst (as suggested by the clustering of GRB spectral peaks at $\epsilon \sim 1$, see Preece et al. 2000) there should exist a strong correlation between t_{peak} and the observed isotropic energy E of the prompt GRB.
4. In the massive progenitor scenario, the prompt high-energy γ -rays must be absorbed efficiently by radiation scattered in the wind. As a result, the high-energy tail of the GRB will have a break whose position is given by equation (82). Time-resolved spectroscopy should show a break at modest energies ~ 10 MeV in the beginning of the GRB and its slow shift to higher energies with time. Once the break is observed one can evaluate the density of the wind.

The main observational effect of the radiation front is the strong softening of the early blast wave emission (which would be otherwise in the hard X-ray band). Owing to this softening the blast wave radiates in a different spectral window compared to the prompt GRB and it can be studied separately in simultaneous observations. Observations in optical – soft X-ray bands at early times (less than ~ 1 min) can help to establish the nature of the GRB progenitor – as we discussed here a wind from a massive progenitor should have clear signatures.

Early optical emission has already been detected in GRB 990123 (Akerlof et al. 1999) and it likely comes from the external shock rather than internal dissipation in the ejecta since there is no correlation between the optical light curve and the prompt GRB. The optical emission can be produced by the reverse shock in the ejecta (e.g. Sari & Piran 1999). The results of the present paper suggest an alternative interpretation:

the soft emission is produced by the forward shock of the blast wave at early stages when it propagates in the preaccelerated and pair-loaded environment. In both models one needs to explain the irregular shape of the optical light curve observed in GRB 990123. E.g. it could be due to inhomogeneous density profile of the medium.

Note that the blast wave emission hardens with increasing R when it moves in the e^\pm loaded zone $R < R_{\text{load}}$ and the observer will see the whole spectrum from optical to X-ray bands. This broad-band emission can overlap with the prompt GRB and its X-ray component can affect the measured GRB spectrum. In particular, the early external shock may generate the soft X-ray

excesses detected in GRBs.

In this paper, we assumed that the prompt GRB is generated at early stages by internal dissipation inside the ejecta and studied the impact of the radiation front on the external shock. If the GRB itself is produced/triggered by the external shock then one deals with a different self-consistent problem (Beloborodov A.M., in preparation).

I thank A.F. Illarionov and C. Thompson for discussions. This work was supported by the Swedish Natural Science Research Council and RFBR grant 00-02-16135.

APPENDIX

SCATTERING AND PHOTON-PHOTON ABSORPTION

Compton scattering

The differential cross-section for Compton scattering (defined in the electron rest frame) is given by (Jauch & Rohrlich 1976)

$$\frac{d\sigma}{d\tilde{\mu}} = \frac{3}{8} \sigma_T \left(\frac{\tilde{\epsilon}_{\text{sc}}}{\tilde{\epsilon}} \right)^2 \Psi, \quad \Psi = \frac{\tilde{\epsilon}_{\text{sc}}}{\tilde{\epsilon}} + \frac{\tilde{\epsilon}}{\tilde{\epsilon}_{\text{sc}}} - 2(1 - \tilde{\mu}) + (1 - \tilde{\mu})^2, \quad \frac{\tilde{\epsilon}_{\text{sc}}}{\tilde{\epsilon}} = \frac{1}{1 - \tilde{\epsilon}(1 - \tilde{\mu})}, \quad (1)$$

where $\tilde{\epsilon}$ and $\tilde{\epsilon}_{\text{sc}}$ are the photon energies before and after scattering respectively (as measured in the electron rest frame), and $\tilde{\mu}$ is the cosine of the scattering angle in the rest frame. In our problem the scattering medium is cold and has a bulk velocity β parallel to the direction of the primary collimated photons. The rest-frame magnitudes are then related to the lab ones by

$$\tilde{\epsilon} = \gamma(1 - \beta)\epsilon, \quad \tilde{\epsilon}_{\text{sc}} = \gamma(1 - \beta\mu)\epsilon_{\text{sc}}, \quad \tilde{\mu} = \frac{\mu - \beta}{1 - \beta\mu}, \quad \frac{d\sigma}{d\mu} = \frac{d\tilde{\mu}}{d\mu} \frac{d\sigma}{d\tilde{\mu}} = \frac{3}{8} \sigma_T \left(\frac{\epsilon_{\text{sc}}}{\epsilon} \right)^2 \frac{1 + \beta}{1 - \beta} \Psi. \quad (2)$$

The total cross-section is given by

$$\sigma_{\text{KN}} = \frac{3}{8} \frac{\sigma_T}{\tilde{\epsilon}} \left[\left(1 - \frac{2}{\tilde{\epsilon}} - \frac{2}{\tilde{\epsilon}^2} \right) \ln(1 + 2\tilde{\epsilon}) + \frac{1}{2} + \frac{4}{\tilde{\epsilon}} - \frac{1}{2(1 + 2\tilde{\epsilon})^2} \right]. \quad (3)$$

Saturation of radiative acceleration

When the medium accelerates, the typical photon energy in the medium rest frame is redshifted well below $m_e c^2$ and the scattering occurs with Thomson cross-section, $d\sigma/d\tilde{\mu} = (3/8)\sigma_T(1 + \tilde{\mu}^2)$ and $\sigma_{\text{KN}} = \sigma_T$. With increasing γ the finite collimation angle of the radiation intensity $I(\theta)$ becomes important and the efficiency of radiative acceleration drops. The radiative force accelerating the electron is (Gurevich & Rumyantsev 1965)

$$\frac{dp}{dt} = \frac{\sigma_T}{c} \gamma^2 [I_1(1 + \beta^2) - (I_0 + I_2)\beta], \quad I_k = \int I(\theta) \cos^k \theta d\Omega. \quad (4)$$

Here θ is the angle between the ray and the radial direction. Note that the net flux $F = I_1$. If the radiation field is perfectly collimated ($I_0 = I_1 = I_2 = F$) then $dp/dt = (\sigma_T/c)F(1 - \beta)/(1 + \beta)$. For a finite collimation there exists a frame with velocity β_{sat} where the radiation flux vanishes. Assume that radiation is isotropic in this frame and has moments $\hat{I}_1 = 0$ and $\hat{I}_2 = \hat{I}_0/3$. The I_k represent the components of the stress-energy tensor of radiation, $\hat{I}_0 = cT^{00}$, $I_1 = cT^{0x}$, $I_2 = cT^{xx}$ (the x -axis is chosen along the radial direction). From the corresponding transformation law ($T^{ik} = \hat{T}^{lm}\Lambda_l^i\Lambda_m^k$ where Λ is the Lorentz matrix) one gets

$$I_0 = \left(1 + \frac{\beta_{\text{sat}}^2}{3} \right) \gamma_{\text{sat}}^2 \hat{I}_0, \quad I_1 = \frac{4}{3} \beta_{\text{sat}} \gamma_{\text{sat}}^2 \hat{I}_0, \quad I_2 = \left(\frac{1}{3} + \beta_{\text{sat}}^2 \right) \gamma_{\text{sat}}^2 \hat{I}_0. \quad (5)$$

Using these relations we get

$$\frac{dp}{dt} = \frac{\sigma_T F}{c} \frac{\gamma^2}{\beta_{\text{sat}}} (\beta_{\text{sat}} - \beta)(1 - \beta\beta_{\text{sat}}) \approx \frac{\sigma_T F}{c} \left(\frac{1 - \beta}{1 + \beta} \right) \left[1 - \frac{(1 - \beta_{\text{sat}})^2}{(1 - \beta)^2} \right] \approx \frac{\sigma_T F}{c} \left(\frac{1 - \beta}{1 + \beta} \right) \left(1 - \frac{\gamma^4}{\gamma_{\text{sat}}^4} \right), \quad (6)$$

where the approximate equalities make use of $\gamma_{\text{sat}} \gg 1$.

$\gamma - \gamma$ absorption

The $\gamma - \gamma$ opacity seen by a scattered photon $(\mu, \epsilon_{\text{sc}})$ is given by

$$\kappa_{\gamma\gamma}(\mu, \epsilon_{\text{sc}}) = \int_{\epsilon_{\text{thr}}}^{\epsilon_{\text{br}}} \frac{F_\epsilon \sigma_{\gamma\gamma}}{m_e c^3 \epsilon} d\epsilon, \quad \epsilon_{\text{thr}} = \frac{2}{(1-\mu)\epsilon_{\text{sc}}}, \quad (7)$$

where $\sigma_{\gamma\gamma}$ is the cross section for $\gamma - \gamma$ pair production (Jauch & Rohrlich 1976)

$$\sigma_{\gamma\gamma}(\epsilon_c) = \frac{3\sigma_T}{8\epsilon_c^2} \left[\left(2 + \frac{2}{\epsilon_c^2} - \frac{1}{\epsilon_c^4} \right) \ln \left(\epsilon_c + \sqrt{\epsilon_c^2 - 1} \right) - \left(1 + \frac{1}{\epsilon_c^2} \right) \sqrt{1 - \frac{1}{\epsilon_c^2}} \right]. \quad (8)$$

Here $\epsilon_c = (\epsilon/\epsilon_{\text{thr}})^{1/2}$ is the energy of the interacting photons in their center-of-momentum frame. The mean energy of the photon absorbed by our photon $(\mu, \epsilon_{\text{sc}})$ is

$$\epsilon_{\text{abs}}(\mu, \epsilon_{\text{sc}}) = \int_1^{\sqrt{\epsilon_{\text{br}}/\epsilon_{\text{thr}}}} \epsilon(\epsilon_c) P(\epsilon_c) d\epsilon_c = \chi \epsilon_{\text{thr}}, \quad P(\epsilon_c) d\epsilon_c = \frac{F_\epsilon \sigma_{\gamma\gamma}(\epsilon_c) d\ln \epsilon_c}{\int_1^{\sqrt{\epsilon_{\text{br}}/\epsilon_{\text{thr}}}} F_\epsilon \sigma_{\gamma\gamma}(\epsilon_c) d\ln \epsilon_c}. \quad (9)$$

Here $P(\epsilon_c)$ is the probability of $\gamma - \gamma$ interaction with given ϵ_c and $\epsilon(\epsilon_c) = \epsilon_{\text{thr}} \epsilon_c^2$. Thus defined numerical factor χ depends on the spectrum shape F_ϵ . If the absorbing radiation has a power-law spectrum $F_\epsilon = F_1 \epsilon^{-\alpha}$ one gets at $\epsilon_{\text{thr}} \ll \epsilon_{\text{br}}$

$$\kappa_{\gamma\gamma} = \frac{\hat{\phi}(\alpha)}{\lambda_1} \left(\frac{\epsilon_{\text{thr}}}{2} \right)^{-\alpha}, \quad \hat{\phi}(\alpha) = 2^{1-\alpha} \int_1^\infty \frac{\sigma_{\gamma\gamma}}{\sigma_T} \epsilon_c^{-2\alpha-1} d\epsilon_c, \quad \chi = \frac{\hat{\phi}(\alpha-1)}{2\hat{\phi}(\alpha)}, \quad (10)$$

where $\lambda_1 = m_e c^3 / F_1 \sigma_T$. The numerical factor $\hat{\phi}(\alpha)$ is with high accuracy ($< 0.3\%$ for $0 < \alpha < 6$) approximated as $\hat{\phi}(\alpha) = (7/12) 2^{-\alpha} (1+\alpha)^{-5/3}$ [Svensson 1987, eq. B6 where $\eta = 2^{\alpha+1} (\alpha+2)^{-1} \hat{\phi}$]. It gives $\chi = (1+\alpha^{-1})^{5/3}$.

The mean energy and momentum of the e^\pm pair created when the scattered photon gets absorbed are

$$e_\pm(\mu, \epsilon_{\text{sc}}) = (\epsilon_{\text{sc}} + \epsilon_{\text{abs}}) m_e c^2, \quad p_\pm(\mu, \epsilon_{\text{sc}}) = (\mu \epsilon_{\text{sc}} + \epsilon_{\text{abs}}) m_e c. \quad (11)$$

In the rest frame of the medium, the average Lorentz factor and momentum per injected particle are given by Lorentz transformation of the energy-momentum vector,

$$2m_e c^2 \gamma_{\text{inj}}(\mu, \epsilon_{\text{sc}}) = \gamma (e_\pm - \beta c p_\pm), \quad 2p_{\text{inj}}(\mu, \epsilon_{\text{sc}}) = \gamma \left(p_\pm - \beta \frac{e_\pm}{c} \right). \quad (12)$$

Integrating over the whole primary spectrum and scattering angles, one can get the mean γ_{inj} and p_{inj} .

The effective Klein-Nishina cutoff

To the first order, $\epsilon_{\text{KN}} \sim \gamma(1+\beta)$. This estimate is sufficient if $\epsilon_{\text{KN}} \gg 1$, far from the spectrum peak. However at $\gamma \sim 1$ we have ϵ_{KN} near the peak and the results of the analytical model in § 5 are sensitive to the exact position of ϵ_{KN} . The effective ϵ_{KN} depends on what we calculate. In calculations of \dot{n}_+ (eq. 8 of the paper), $d\sigma$ enters in combination with $\kappa_{\gamma\gamma}$ seen by the scattered photon. Let us assume $\beta = 0$ and compute the average

$$\sigma_{\text{KN}} \overline{\kappa_{\gamma\gamma}}(\epsilon) = \int d\sigma \kappa_{\gamma\gamma}(\mu, \epsilon_{\text{sc}}) = \frac{\sigma_T}{\lambda_1} \hat{\phi}(\alpha_2) \epsilon^{\alpha_2} X_{\alpha_2}(\epsilon), \quad X_\alpha \equiv \overline{\left[(1-\mu) \frac{\epsilon_{\text{sc}}}{\epsilon} \right]^\alpha} = \frac{\sigma_{\text{KN}}}{\sigma_T} \int_{-1}^1 d\mu \frac{d\sigma}{d\mu} \left[(1-\mu) \frac{\epsilon_{\text{sc}}}{\epsilon} \right]^\alpha. \quad (13)$$

Here bar denotes the averaging over scattering angles. At $\epsilon \ll 1$ we are in the Thomson regime with $X_\alpha = X_\alpha^T = (3/8) \int (1-\mu)^\alpha (1+\mu^2) d\mu$, e.g. $X_2^T = 7/5$. The Klein-Nishina correction factor is important ($\sim 1/2$) already at $\epsilon \sim 0.1$. This is caused by two effects: (1) the scattering angle is reduced [and $\kappa_{\gamma\gamma} \propto (1-\mu)^{\alpha_2}$] and (2) the total cross-section σ_{KN} is reduced. Photons of energy $(\epsilon, \epsilon + d\epsilon)$ contribute to \dot{n}_+ with approximate weight $\propto (F_\epsilon/\epsilon) \sigma_{\text{KN}} \overline{\kappa_{\gamma\gamma}}$ (see eq. 8 of the paper), therefore we define the effective ϵ_{KN} for pair loading as

$$\int_0^\infty d\epsilon \frac{F_\epsilon}{\epsilon} \epsilon^{\alpha_2} X_{\alpha_2} = \int_0^{\epsilon_{\text{KN}}} d\epsilon \frac{F_\epsilon}{\epsilon} \epsilon^{\alpha_2} X_{\alpha_2}^T, \quad \epsilon_{\text{KN}} = \left[(\alpha_2 - \alpha_1) \int_0^\infty d\epsilon f_\epsilon \epsilon^{\alpha_2-1} \frac{X_{\alpha_2}}{X_{\alpha_2}^T} \right]^{1/(\alpha_2-\alpha_1)} \approx 0.4, \quad (14)$$

where $f_\epsilon \equiv F_\epsilon/F_1$. We get $\epsilon_{\text{KN}} \approx 0.4$ for $\alpha_1 = 0$ and $\alpha_2 = 1.5, 2, 2.5$.

When calculating \dot{P}_\pm (eq. 18 of the paper), we need to evaluate

$$\sigma_{\text{KN}} \overline{\kappa_{\gamma\gamma} p_\pm}(\epsilon) = \int d\sigma \kappa_{\gamma\gamma}(\mu, \epsilon_{\text{sc}}) p_\pm \approx \frac{\sigma_T}{\lambda_1} \hat{\phi}(\alpha_2 - 1) \epsilon^{\alpha_2-1} X_{\alpha_2-1}(\epsilon), \quad (15)$$

where we neglected the $\overline{\kappa_{\gamma\gamma}\mu\epsilon_{sc}}$ term in $\overline{\kappa_{\gamma\gamma}p_{\pm}}$. Photons of energy $(\epsilon, \epsilon + d\epsilon)$ contribute to \dot{P}_{\pm} with approximate weight $\propto (F_{\epsilon}/\epsilon)\sigma_{KN}\overline{\kappa_{\gamma\gamma}p_{\pm}}$ (see eq. 18 of the paper), and the effective ϵ_{KN} is given by

$$\int_0^{\infty} d\epsilon \frac{F_{\epsilon}}{\epsilon} \epsilon^{\alpha_2-1} X_{\alpha_2} = \int_0^{\epsilon_{KN}} d\epsilon \frac{F_{\epsilon}}{\epsilon} \epsilon^{\alpha_2-1} X_{\alpha_2-1}^T, \quad \epsilon_{KN} = \left[(\alpha_2 - \alpha_1 - 1) \int_0^{\infty} d\epsilon f_{\epsilon} \epsilon^{\alpha_2-2} \frac{X_{\alpha_2-1}}{X_{\alpha_2-1}^T} \right]^{\frac{1}{\alpha_2 - \alpha_1 - 1}} \approx 0.4. \quad (16)$$

We assumed here that $\alpha_2 - \alpha_1 > 1$. Again we get $\epsilon_{KN} \approx 0.4$ for $\alpha_1 = 0$ and $\alpha_2 = 1.5, 2, 2.5$.

In a similar way, one can estimate the effective ϵ_{KN} for \dot{P}_{sc} (see eq. 17 of the paper),

$$\sigma_{KN} \overline{(1 - \mu \frac{\epsilon_{sc}}{\epsilon})} = \sigma_T Z, \quad \int_0^{\infty} d\epsilon F_{\epsilon} Z = \int_0^{\epsilon_{KN}} d\epsilon F_{\epsilon} Z^T, \quad \epsilon_{KN} = \int_0^{\infty} d\epsilon f_{\epsilon} \frac{Z}{Z^T} \sim 0.7. \quad (17)$$

Here $Z^T = (1 + \beta)^{-1}$.

REFERENCES

Akerlof, C. et al. 1999, *Nature*, 398, 400
 Blandford, R. D., & McKee, C. F. 1977, *MNRAS*, 180, 343
 Chevalier, R. A., & Li, Z.-Y. 1999, *ApJ*, 520, L29
 Dermer, C. D., & Böttcher, M. 2000, *ApJ*, 534, L155
 Gurevich, L. E., & Rumyantsev, A. A., 1965, *Sov. Physics – JETP*, 20, 1233
 Jauch, J. M., & Rohrlich, F. 1976, *The Theory of Photons and Electrons*, Springer, New York
 Mészáros, P., Ramirez-Ruiz, E., & Rees, M. J. 2000, *astro-ph/0011284*
 Madau, P., & Thompson, C. 2000, *ApJ*, 534, 239
 Piran, T. 1999, *Phys. Rep.*, 314, 575
 Preece, R. D., Briggs, M. S., Mallozzi, R. S., Pendleton, G. N., Paciesas, W. S., & Band, D. L. 2000, *ApJS*, 126, 19
 Rees, M. J., & Mészáros, P. 1992, *MNRAS*, 258, 41
 Sari, R., & Piran, T. 1999, *ApJ*, 517, L109
 Svensson, R. 1987, *MNRAS*, 227, 403
 Thompson, C., & Madau, P. 2000, *ApJ*, 538, 105 (TM)
 Woosley, S. E. 1993, *ApJ*, 405, 273